

Alpha-synuclein interacts with regulators of ATP homeostasis in mitochondria

Received: 31 January 2024

Accepted: 1 August 2025

Published online: 16 August 2025

 Check for updates

Tetiana Serdiuk^{1,5}, Yanick Fleischmann^{2,5}, Dhiman Ghosh², Aro Delparente³, Viviane Reber¹, Larissa Frey², David Rhyner², Juan Gerez², Norbert Volkmar¹, Lucie Kralickova¹, Guillaume Mas⁴, Christian Dörig¹, Sebastian Hiller⁴, Roger Schibli³, Linjing Mu³, Paola Picotti¹✉ & Roland Riek²✉

Mitochondrial dysfunction and accumulation of α -synuclein aggregates are hallmarks of the neurodegenerative Parkinson's disease and may be interconnected. To investigate the interplay between α -synuclein and brain mitochondria at near atomic structural level, we apply NMR and identify α -synuclein protein interactors using limited proteolysis-coupled mass spectrometry (LiP-MS). Several of the proteins identified are related to ATP synthesis and homeostasis and include subunits of ATP synthase and the adenylate kinase AK2. Furthermore, our data suggest that α -synuclein interacts with the Parkinson's disease-related protein DJ1. NMR analysis demonstrates that both AK2 and DJ1 bind to the C-terminus and other segments of α -synuclein. Using a functional assay for AK2, we show that monomeric α -synuclein has an activating effect, whereas C-terminally truncated α -synuclein and α -synuclein in an amyloid fibrillar state have no significant effect on AK2 activity. Our results suggest that α -synuclein modulates ATP homeostasis in a manner dependent on its conformation and its C-terminal acidic segment.

Parkinson's disease (PD) is among the most common neurodegenerative diseases, and the likelihood that a person will develop PD increases with age^{1–3}. PD is classified as an α -synucleinopathy. These are diseases characterized by the presence of aggregates of α -synuclein (α Syn) in neurons, nerve fibers, or glial cells⁴. α Syn is a small, 140-residue-long protein that is intrinsically disordered in mammalian cells⁵. Several point mutations of α Syn, as well as duplications and triplications of the *SNCA* gene, which encodes α Syn, are known to be correlated with an increased probability of early-onset PD^{6,7}. The first roughly 100 residues of α Syn can form amphipathic helices capable of binding to lipid membranes with a preference for negatively charged phospholipids⁸. Furthermore, α Syn has a preference for mitochondrial membranes, possibly due to the high cardiolipin content^{9,10}.

The role of the mitochondria in PD has been the subject of intense PD-related research. Environmental and genetic links between PD and

mitochondrial dysfunction have been established^{11,12}. Mitochondria support neuronal activity and are actively transported within neurons toward locations where ATP is required¹³. Mitochondrial dysfunction is a hallmark of not only PD but also of other neurodegenerative diseases, including Alzheimer's disease and prion diseases^{14,15}. Transplantation of healthy mitochondria has been proposed as a potential treatment for PD^{16,17}.

The interaction between α Syn and the mitochondrial membrane alters the membrane curvature and is important for the fusion and fission of mitochondria^{18,19}. The N-terminus and the non-amyloid β -component (NAC) region of α Syn are critical for the interaction with the membrane^{19,20}. Expression of α Syn with a disrupted N-terminal domain leads to elongated mitochondria²¹. In addition to interacting with the outer mitochondrial membrane, α Syn is also found in the intermembrane mitochondrial space (IMS)²². Several import-related

¹Institute of Molecular Systems Biology, ETH Zürich, Zürich, Switzerland. ²Institute of Molecular Physical Science, ETH Zürich, Zürich, Switzerland.

³Department of Chemistry and Applied Biosciences, ETH Zürich, Zürich, Switzerland. ⁴Biozentrum, University of Basel, Basel, Switzerland. ⁵These authors contributed equally: Tetiana Serdiuk, Yanick Fleischmann. ✉e-mail: picotti@imsb.biol.ethz.ch; roland.riek@phys.chem.ethz.ch

proteins, namely VDAC^{23,24}, Tom40^{25,26}, and Tom20²⁷ were shown to interact with α Syn. Once in the IMS, α Syn is mostly associated with the inner mitochondrial membrane (IMM), possibly this binding is electrostatically driven due to the high content of negatively charged cardiolipin^{26,28}.

Multiple lines of evidence underscore the significance of the α Syn-mitochondria interaction in the pathogenesis of PD. For example, α Syn and mitochondria co-localize in cells that overexpress α Syn²⁹. Damaged mitochondria and α Syn are found in Lewy bodies³⁰. Moreover, increased α Syn translocation to the mitochondria is observed in cells with abnormally low cytosolic pH or upon depletion or inhibition of the chaperones Hsc70 and Hsp90, conditions that induce α Syn aggregation^{31,32}. Mitochondrial accumulation of α Syn impairs the function of complex I and reduces mitochondrial activity²⁶. Additionally, oligomeric species of α Syn prevent mitochondrial protein import^{25,27}.

How α Syn aggregation influences mitochondrial function remains not fully understood. It has been suggested that mitochondrial dysfunction occurs prior to α Syn aggregation and that α Syn translocation and aggregation occur as a result of aberrations in mitochondrial function³³. Translocation of α Syn to the mitochondria could result from cellular degeneration or due to a rescue response. It remains of vital importance to distinguish pathological processes from normal functions of α Syn in mitochondria.

In this work, we aim to characterize interactions between α Syn and the mitochondrial proteome and assess their potential physiological or pathological implications. We use mitochondria isolated from bovine brain white matter and incubate them with monomeric WT α Syn, C-terminally truncated α Syn, or α Syn fibrils and analyze these samples using limited proteolysis-coupled mass spectrometry (LiP-MS), an unbiased technique capable of detecting protein interactions and proteome-wide changes in conformation^{34,35}. We use NMR to study the interactions of selected proteins on a structural level and evaluate the impacts of α Syn on the enzymatic function of mitochondrial proteins.

Results

α Syn interacts with membranes and proteins of isolated brain mitochondria

For our studies, we used mitochondria isolated from the white matter of the bovine brain, as these mitochondria mostly originate from axons, which are believed to be relevant in α Syn-related diseases such as PD³⁶. A mitochondria-enriched fraction was extracted by stepwise centrifugation of minced white matter. To confirm that the fraction contained intact and active mitochondria, a luciferase-based bioluminescence assay was performed to measure the rate of ATP synthesis by mitochondria supplied with metabolites crucial to the respiratory chain. The light emission detected in the assay is proportional to the ATP produced by the mitochondria due to the rapid conversion of ATP by luciferase during oxidation of its substrate luciferin (Supplementary Fig. 1a). Due to the presence of adenylate kinases in the mitochondria-enriched fraction, the presence of ATP generation alone does not per se mean that mitochondria are intact. Here, we use different combinations of supplemented metabolites, which allows monitoring of respiratory chain complexes that are dependent on an intact inner mitochondrial membrane³⁷. In mitochondria-enriched fractions, ATP was produced over time, and the rate of ATP synthesis was higher in samples supplemented with either glutamate/malate or pyruvate/malate (Supplementary Fig. 1b). These metabolites provide a carbon source to the citric acid cycle, which results in the production of NADH. The NADH is, in turn, oxidized by complex I, resulting in a proton gradient across the inner mitochondrial membrane³⁷. This gradient, which only persists in intact mitochondria, is essential for the production of ATP by the ATP synthase. The higher rate of ATP production upon metabolite supplementation was indicative of active and intact mitochondria.

We first used liquid-state NMR to directly study α Syn concentration and localization in mitochondria preparations. Mitochondria were incubated in a solution containing recombinantly expressed ¹⁵N-labeled, monomeric, N-terminally acetylated human wild-type (WT) α Syn (20 μ M). The mitochondria were washed until the supernatant was free of α Syn (Supplementary Fig. 2a). Analysis of a ¹⁵N-filtered 1D ¹H NMR experiment (i.e., the first time increment of a [¹⁵N-¹H]-HMQC NMR spectrum) revealed that α Syn was captured in the mitochondrial fraction (Supplementary Fig. 2b). The concentration of soluble α Syn in the mitochondrial fraction was estimated to be $2 \pm 0.5 \mu$ M by comparing the signal intensity in this preparation to a sample of ¹⁵N-labeled α Syn in buffer (Supplementary Fig. 2c).

To determine whether α Syn transiently interacts with mitochondrial proteins and membranes, we monitored chemical shifts and cross-peak intensities of ¹⁵N-labeled α Syn in the absence and the presence of lysed bovine mitochondria. We carried out 2D [¹⁵N,¹H] HMQC NMR experiments, chemical shift perturbations (CSPs), and signal loss analyses. A change of chemical shifts indicates an interaction with another molecule. If the interaction is of a transient nature in the order of micro- to milliseconds, the signal is lost because the chemical shift changes between binding to non-binding are in the order of the NMR time scale of measurement, yielding faster relaxation of the NMR signal.

In the presence of lysed mitochondria, the signal intensity of cross peaks between α Syn residues was reduced by around 60% for the first 100 residues with less dramatic reductions toward the C-terminus compared to ¹⁵N-labeled α Syn in buffer (Fig. 1a). Chemical shift differences were roughly equally distributed over the sequence with the largest differences in residues 100 to 115 (Fig. 1b). These findings indicate that transient interactions occur between α Syn and mitochondria membranes and/or proteins.

Previous work has shown that α Syn associates with the inner mitochondrial membrane through interactions with the doubly negatively charged lipid cardiolipin⁸. Although not the only negatively charged lipid in the inner membrane, cardiolipin is highly abundant in the mitochondrial membrane³⁸. To mimic the mitochondrial inner membrane, we embedded cardiolipin in the lipid bilayer mimetic nanodiscs and compared the peak intensity ratios and CSPs of α Syn in the presence and absence of these nanodiscs. The peak intensities of α Syn residues in the N-terminal region were reduced in the presence of cardiolipin compared to its absence, but the presence of cardiolipin had little to no effect on residues near the C-terminus (Fig. 1a). Moreover, all significant perturbations in chemical shift were near the N-terminus (Fig. 1b). Similar observations were previously reported for transient interactions of the positively charged N-terminal segment of α Syn with negatively charged lipid membranes^{8,39}. The results with the membrane-mimicking system differed from those with lysed mitochondria. We assume that the signal decrease and CSPs near the N-terminus of α Syn in the presence of the lysed mitochondria are due to an interaction with the negatively charged membrane. In addition to these changes, lysed mitochondria also caused significant changes in the NAC region and the C-terminal region. The NAC region (61–95 aa) is of interest due to its important role in α Syn aggregation⁴⁰.

AK2 and ATP synthase interact with α Syn

To determine whether the changes in the NMR spectra of α Syn in the presence of mitochondria might be due to interactions with specific mitochondrial proteins, we applied LiP-MS^{41,42}, an approach that detects local and global protein structural alterations, including protein-protein interactions, protein-small molecule interactions, protein aggregation, conformational changes, and post-translational modifications (PTMs) directly from complex biological samples on a proteome-wide scale. LiP-MS was recently used to detect interactors of purified proteins, including intrinsically disordered proteins, added to complex cell extracts, based on alterations of proteolytic patterns of

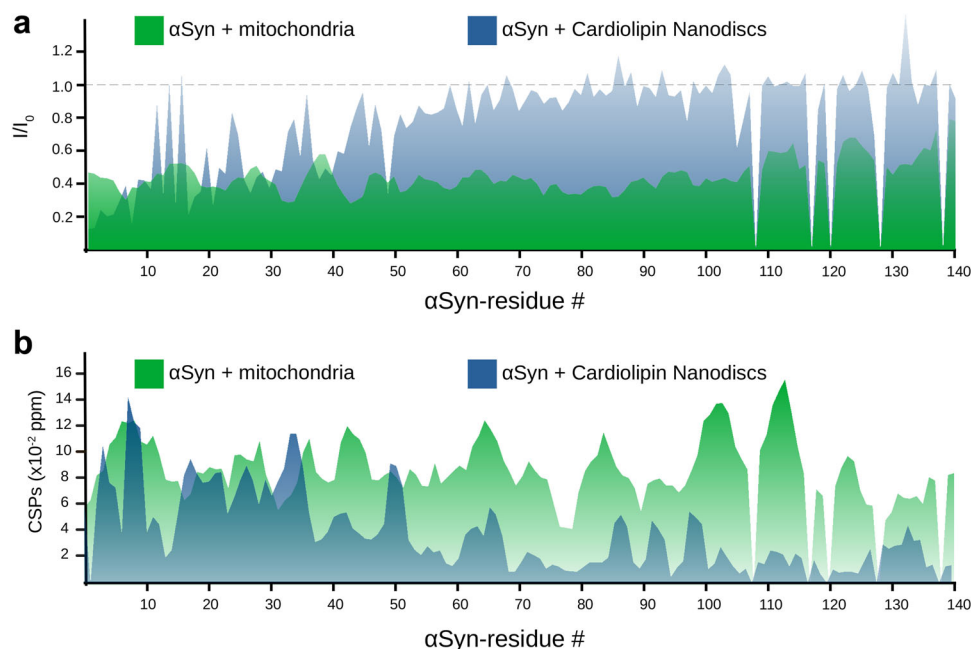


Fig. 1 | Transient residue-resolved interaction of mitochondria with αSyn.

Comparison between the chemical shift perturbations and intensity changes of αSyn caused by interaction with either lysed bovine mitochondria (green) or cardiolipin nanodiscs (blue). The data is presented as a rolling average of three points. Peak positions and peak intensities are extracted from 2D [^{15}N , ^1H] HMQC NMR spectra. **a** Intensity ratios of peaks in the presence (I) and absence (I_0) of nanodiscs or lysed bovine brain mitochondria. **b** Chemical shift perturbations (CSPs) of peaks in the presence and absence of nanodiscs or lysed bovine brain mitochondria.

a, b The interaction with lipid membrane nanodiscs appears to influence the N-terminal region of αSyn, indicating an interaction between the positively charged N-terminal segment of αSyn with the negatively charged cardiolipin, as expected¹⁰, with the second half of the sequence showing no changes. The interaction with mitochondria causes relevant changes in all regions of the sequence, indicating multiple transient interactions that may include membrane interactions. Source data are provided as a Source Data file.

the interacting proteins⁴². Bovine brain mitochondrial lysates were treated either with monomeric WT αSyn for 15 min or with an equal volume of buffer; each condition was evaluated in quadruplicate. Mitochondrial proteomes were digested for a short time under native conditions with the sequence-unspecific protease proteinase K (PK), and the resulting protein fragments were denatured and further digested with trypsin to generate peptides amenable to mass spectrometry analysis. Peptide mixtures were analyzed by liquid chromatography coupled with data-independent acquisition mass spectrometry (DIA, LC-MS/MS). Limited digestion patterns of mitochondrial proteins that interact with αSyn are expected to differ in treated extracts relative to untreated extracts due to altered protease accessibility of interaction sites (Fig. 2a). We detected 22,141 peptides from 3055 different proteins. Of these, 18 proteins differed significantly (q -value lower than 0.05 and fold change larger than 1.5) in their proteolytic patterns in the presence of αSyn (Fig. 2b). Among these candidates were four mitochondrial proteins related to energy metabolism and respiration, namely ATP synthase subunit α (ATPA), AK2, NUDT13, and NDUFB3 (Supplementary Fig. 3). In addition, five peptides from αSyn significantly differed between the two conditions.

The top protein hit (lowest q -value) was the adenylate kinase AK2 (Fig. 2b). Specifically, peptide $^{94}\text{NGFLDGFPR}^{103}$ spanning residues 94–103 of AK2 (aa positions are given for human AK2) was significantly altered and proteolytically protected upon addition of αSyn, suggesting that this region could be an interaction site between αSyn and AK2. Adenylate kinases are proteins that convert two ADP molecules to one ATP and one AMP molecule and vice versa⁴³. Whereas most isoforms are cytosolic, three isoforms, AK2, AK3, and AK4, are mitochondrial; AK3 and AK4 are found in the mitochondrial matrix, and AK2 in the intermembrane space⁴⁴. AK2 uses imported AMP to produce ADP that is translocated into the matrix, where it is used as substrate by ATP synthase⁴⁴. Thus, AK2 is an important player in the energy

homeostasis of mitochondria. Interestingly, another protein crucial for mitochondrial energy production, the α-subunit of the ATP synthase complex, was also structurally altered upon addition of αSyn to the mitochondrial extract (Fig. 2b), further strengthening the link between αSyn and ATP homeostasis. Notably, previous studies have reported physiological⁴⁵ and pathological⁴⁶ relationships between αSyn and the ATP synthase. The α-subunit of the ATP synthase complex binds ADP, and therefore the structural change observed in our LiP-MS screen may originate either from direct interaction of the α-subunit of the ATP synthase with αSyn, or from indirect effect of αSyn on, e.g., AK2 functional activity, which in turn would shift the balance between adenine nucleotides.

Although AK2 is weakly expressed in the brain⁴⁷, it is detected in the substantia nigra, and AK2 expression levels are downregulated in this region in the later stages of PD⁴⁸. To validate these potential physical interactors of αSyn with AK2 and to assess whether these interactions occur also in the context of human cells, we applied affinity-purification coupled to mass spectrometry to lysates of SH-SY5Y human neuroblastoma cells. Monomeric WT αSyn was incubated with SH-SY5Y full-cell lysates, and then αSyn and its bound interactors were immunoprecipitated and analyzed by mass spectrometry. In agreement with our LiP-MS results, both AK2 and the α-subunit of ATP synthase were immunoprecipitated with αSyn (Fig. 2c, affinity purification mass spectrometry (AP-MS)). In total, 177 mitochondrial proteins were immunoprecipitated with monomeric WT αSyn. Among adenylate kinases, in parallel to AK2, we detected AK4, another mitochondrial adenylate kinase, immunoprecipitating with αSyn. Furthermore, we detected multiple subunits of ATP synthase immunoprecipitated with αSyn, namely subunit beta, delta, epsilon pseudogene 2, peripheral stalk subunit OSCP, peripheral stalk subunit d, in addition to subunit alpha, suggesting that the entire ATP synthase complex was immunoprecipitated with αSyn

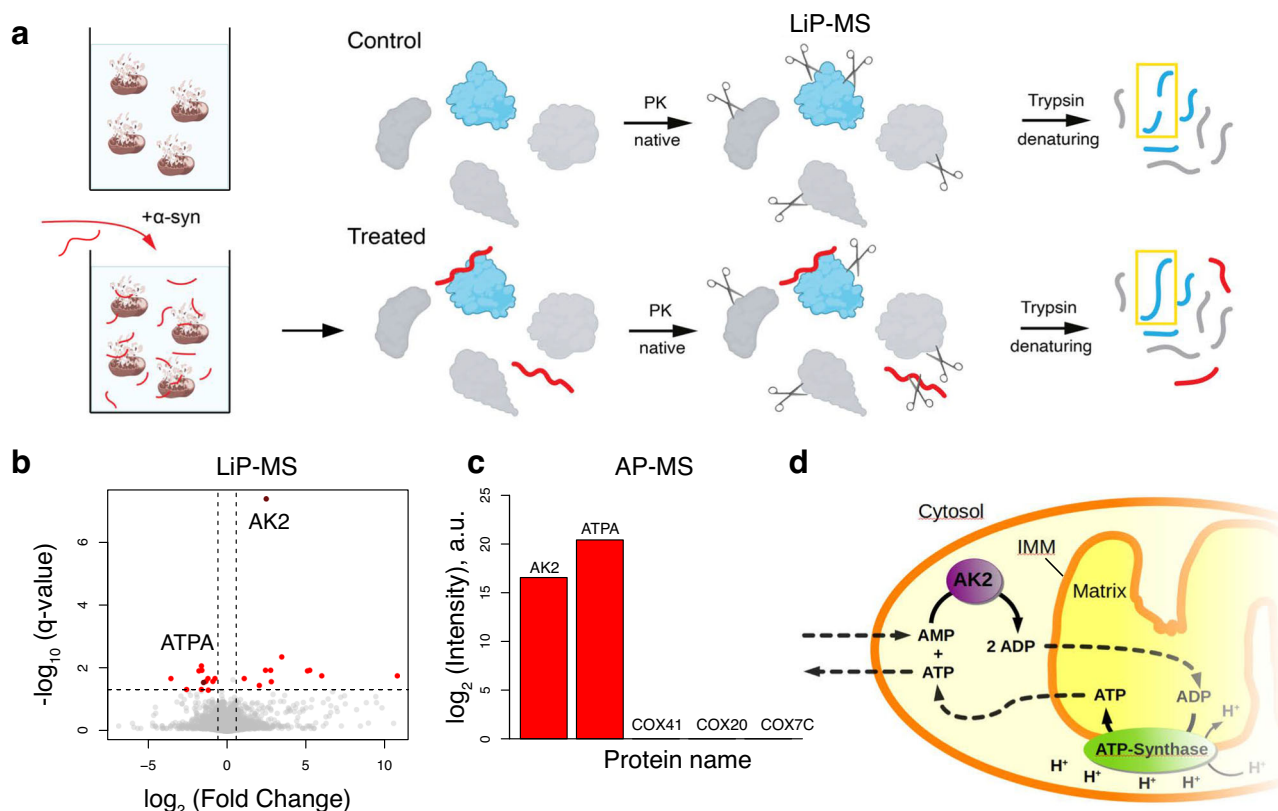


Fig. 2 | Identification of α Syn interaction partners from the mitochondrial proteome determined by LiP-MS. LiP-MS of bovine brain mitochondrial enriched fraction treated with WT α Syn for 15 min. **a** Schematic illustration of the principle of LiP-MS. α Syn-treated and control (untreated) mitochondria were subjected to the LiP-MS workflow. PK was added for 5 min to native mitochondrial proteomes treated and untreated with α Syn. Mitochondrial proteins interacting with α Syn are partially shielded from PK digestion in treated conditions and accessible to PK in untreated conditions. After PK digestion is stopped, proteomes are denatured and digested by trypsin. Peptides are analyzed by LC-MS/MS. Proteins and the regions involved in interaction with α Syn are identified and quantified. Created in BioRender. Picotti

(2025) <https://BioRender.com/051y6yl>; Created in BioRender. Picotti (2025) <https://BioRender.com/wo2308i>. **b** Volcano plot showing LiP-MS peptides reporting on interactions of α Syn with specific proteins. Red dots show statistically significant hits (fold change > 1.5, q -value < 0.05, based on a two-tailed t -test followed by Benjamini–Hochberg adjustment for multiple hypothesis testing). **c** AP-MS validation of AK2 interaction with α Syn monomer. Intensities are shown after subtraction of the background (isotype-specific control). **d** Illustration depicting the role of AK2 in the intermembrane space of the mitochondria. AK2 helps in the recycling of AMP by converting it to ADP, which is transported to the matrix to be used by the ATP-synthase. Source data are provided as a Source Data file.

monomers. Importantly, other mitochondrial proteins such as COX41, COX20, and COX7C were not immunoprecipitated with α Syn (Fig. 2c), indicating that AK2 and ATP synthase, specifically, and not intact mitochondria, were immunoprecipitated with α Syn. Overall, more proteins were immunoprecipitated with α Syn monomers compared to interactors found with LiP-MS, which could be explained by (i) longer incubation times in immunoprecipitation experiments (1 h vs 15 min) and (ii) immunoprecipitation of protein complexes, consisting of direct interactors but also interactors of interactors of α Syn. In summary, in two systems, we identified AK2 and ATP synthase as interactors of α Syn, suggesting an involvement of α Syn in mitochondrial function.

The C-terminus of α Syn is involved in the interaction with AK2

To identify the region of α Syn involved in the interaction with AK2, we compared the peak intensity ratios of 2D [15 N, 1 H] HMQC NMR spectra of 15 N-labeled, N-terminally acetylated, human monomeric WT α Syn in the presence and absence of purified AK2. While in the presence of AK2, some stretches of the N-terminal and NAC regions of α Syn showed intensity decreases relative to α Syn alone, the C-terminal residues 105 to 140 showed stronger decreases of approximately 50% (Fig. 3a).

To verify that the C-terminus of α Syn is the crucial site of interaction with AK2, a LiP-MS experiment was performed with lysed mitochondria incubated with α Syn in the presence or absence of the

bacterial chaperone Skp⁴⁹. Skp binds mainly to the N-terminus of α Syn³¹, and, therefore, Skp was expected to prevent or reduce the binding of mitochondrial proteins that interact with the N-terminus, altering LiP-MS patterns. For many of the 18 significant hits from our first LiP-MS screen (Fig. 2b), the fold change decreased below the threshold, but the LiP-MS pattern of AK2 was not altered by the presence of Skp (Supplementary Fig. 3). This indicated that AK2 likely requires the C-terminus region of α Syn to establish an interaction with the protein. Next, we performed the LiP-MS experiment with a C-terminal-deletion mutant of α Syn (Δ C- α Syn), which includes only residues 1–121 of α Syn. Under these conditions, AK2 was no longer identified as a significant hit (Fig. 3b), indicating that AK2 requires the C-terminal region of α Syn for binding.

To determine whether the binding of α Syn leads to structural changes in AK2, 2D [15 N, 1 H] HMQC spectra of recombinant 15 N-labeled AK2 were collected in the presence and absence of unlabeled, monomeric WT α Syn. The fingerprints of the two spectra, including the number of observed peaks and overall distribution, were similar (Fig. 3c). Most peaks show CSPs, with a handful of them being noticeably stronger than the others. This suggests that there are only subtle secondary structural changes in AK2 due to α Syn binding, while structural changes such as relative domain reorientation may occur. Interestingly, at residues 94–103 at the center of the CORE domain (the peptide ⁹⁴NGFLLDGFPR¹⁰³) was the peptide with abundance significantly altered upon addition of WT α Syn in the LiP-MS experiment,

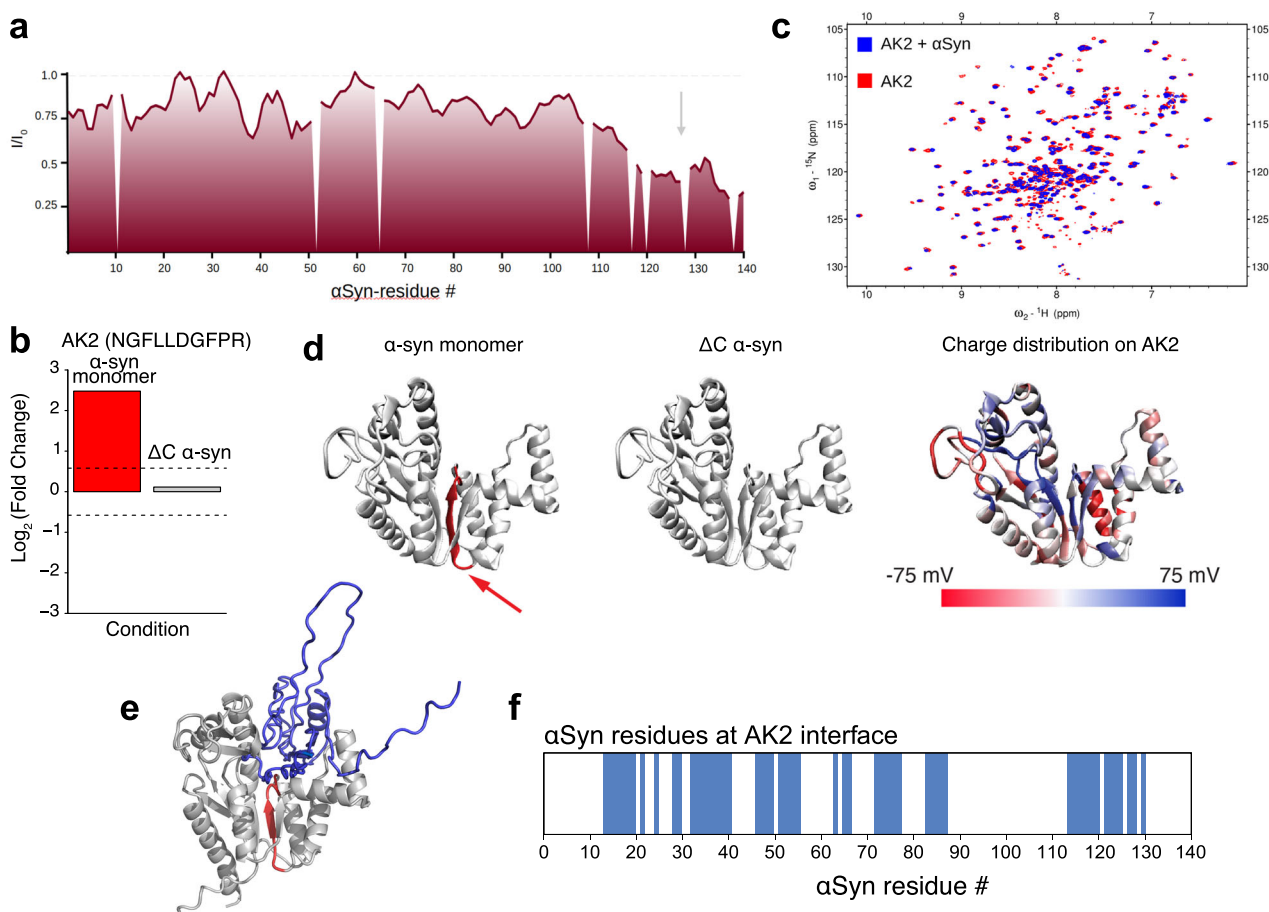


Fig. 3 | The interaction between AK2 and α Syn is facilitated through the C-terminal region of α Syn, affecting widespread small structural changes on AK2, including the hinge region in particular. **a Intensity ratios of α Syn peaks in the presence and absence of AK2 extracted from 2D ^{15}N - ^1H HMQC NMR. A general decrease around the C-terminus indicates binding of this region to AK2. **b** Log_2 (fold change) of AK2 peptide (NGFLLDGFPR) proteolytic protection for α Syn monomer and $\Delta\text{C-}\alpha$ Syn. **c** 2D ^{15}N - ^1H HMQC NMR spectrum of 150 μM ^{15}N -labeled AK2 in the presence (blue) and absence (red) of 200 μM WT α Syn in PBS pH 7.5 at 25 $^\circ\text{C}$. AK2 keeps its folded structure, however, many changes all over the spectrum can be**

seen. **d** Mapping the LiP-MS significant peptide of AK2 to its structure for interactions with WT α Syn monomer and $\Delta\text{C-}\alpha$ Syn. The last panel shows the charge distribution of AK2. **e**, **f** Prediction of interaction between AK2 and α Syn. **e** Alpha-fold 2-based simulation of interactions between AK2 and WT α Syn. AK2 is shown in gray and α Syn in blue. In red is the AK2 peptide that changes in structure in the LiP-MS experiment. Portions of this peptide are at the predicted interaction interface. **f** Mapping the predicted interaction interface of AK2 on the sequence of α Syn. Source data are provided as a Source Data file.

and the abundance of this peptide was unchanged upon addition of $\Delta\text{C-}\alpha$ Syn (Fig. 3d). Residues 95–100 of AK2 form a β -strand, and the next three residues are part of a loop inside the pocket where ATP, ADP, and AMP bind. The β -sheet is directly adjacent to two other β -strands (17–22) and (43–46), with the first β -strand connected to the P-loop that binds the phosphate groups of ATP⁵⁰. Furthermore, the positive charge distribution in the region of these three central β -strands likely favors binding of the acidic α Syn C-terminus (Fig. 3d). Thus, binding of α Syn in this region is likely to have an impact on the activity of AK2. An AlphaFold 2 simulation of the interaction between α Syn and AK2 (Fig. 3e, f and Supplementary Figs. 4 and 5) also suggested the C-terminal region being involved in the interaction with AK2. In addition, several N-terminal segments of α Syn were predicted to bind to AK2 in line with NMR data (Fig. 3a).

α Syn binding increases AK2 activity

In order to study the influence of α Syn binding on the enzymatic activity of AK2, we used a time-resolved 1D ^1H NMR-based activity assay^{46,51,52}. Samples contained the substrates ATP and AMP and monomeric WT α Syn, $\Delta\text{C-}\alpha$ Syn, or α Syn fibrils. α Syn fibrils were prepared and characterized as previously described in ref. 53. Control samples contained no α Syn species. pH adjustment and NMR

experimental set up (such as pulse length calibration, shimming, tuning, and matching) were performed before the addition of AK2, and acquisition began upon the addition of AK2. For each sample, a 1-h pseudo 2D NMR spectrum was recorded, consisting of a series of 1D ^1H NMR spectra. The integrals of the H8 adenine protons of ATP, ADP, and AMP were tracked over time with the one from ADP increasing and those from ATP and AMP decreasing due to the activity of AK2 (Fig. 4a). From the change of the integrals over time a time constant (τ) was extracted that reflects the activity of AK2 and should be dependent on the concentration of added α Syn species (c) if they influence AK2 activity. The results with the time constants in minutes are shown in Fig. 4b. As the concentration of WT α Syn was increased, τ became significantly shorter (3.75 ± 0.38 min for 20 \times excess of α Syn vs 7.3 ± 1.1 min in the absence of α Syn; Fig. 4b). Thus, the presence of WT α Syn increased the enzymatic activity of AK2. There was no significant difference in τ upon addition of $\Delta\text{C-}\alpha$ Syn (Fig. 4b). To confirm these findings, we employed a spectrophotometric AK2 activity assay developed by Song et al.⁵² (Supplementary Fig. 6a). The rate of the reaction catalyzed by AK2 increased in the presence of α Syn but was not significantly altered by the presence of $\Delta\text{C-}\alpha$ Syn (Supplementary Fig. 6b). The α Syn fibrils had no significant effect on AK2 activity (Fig. 4b).

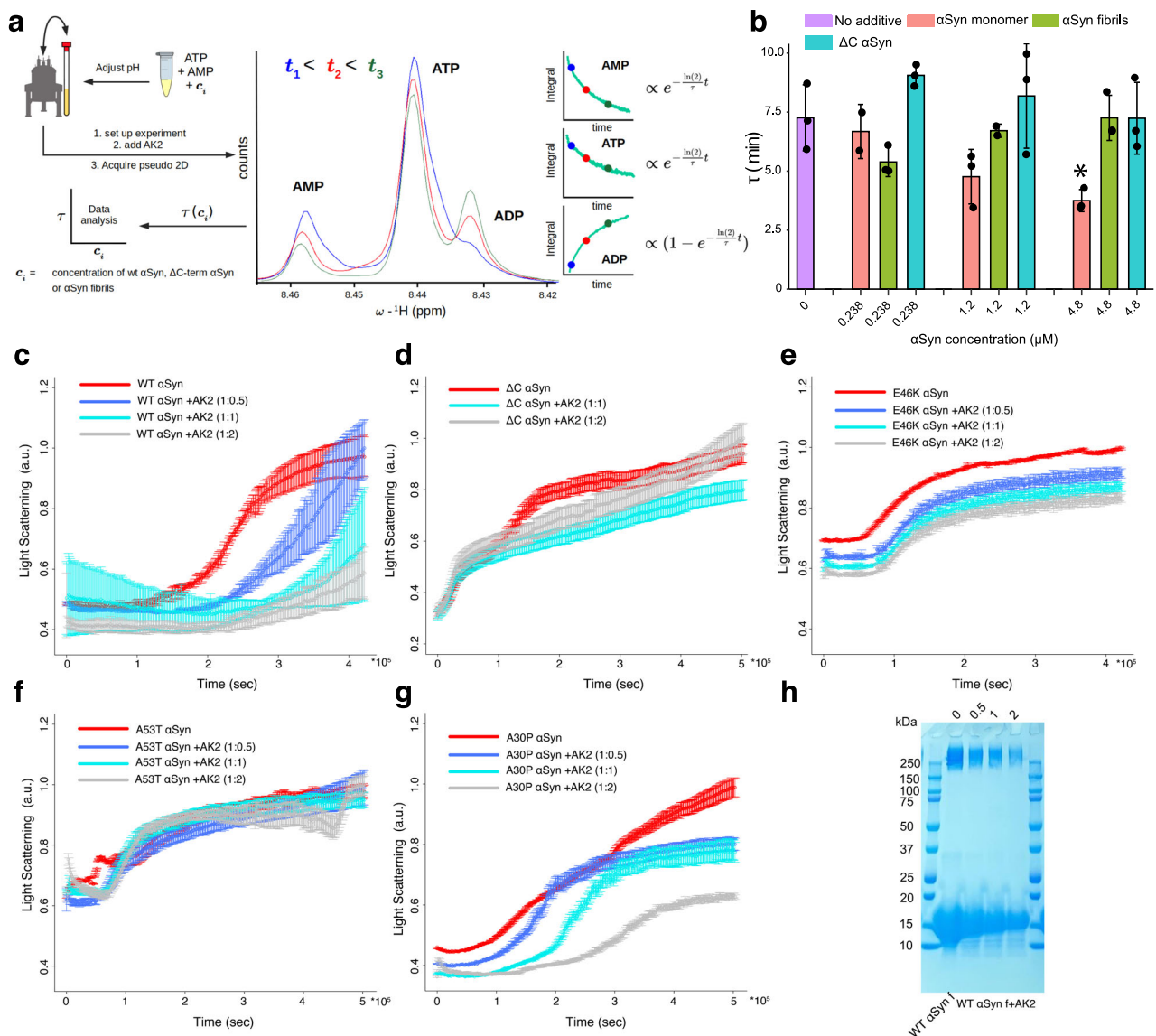


Fig. 4 | α Syn enhances AK2 catalytic activity. 1D proton NMR-based AK2 activity assay in the presence and absence of WT α Syn, α Syn fibrils, or C-terminal truncated α Syn (Δ C- α Syn). **a** Schematic illustration of the principle of the method. A pH-adjusted starting solution of a 1:2 AMP/ATP mixture is treated with AK2 to initiate the reaction. A series of 1D proton NMR spectra as a pseudo-2D are recorded. The intensities of the H8 proton of adenine are extracted and plotted over time. From this, a time constant (τ) is fitted to compare the activity in the presence of different α Syn species. **b** Concentration-dependent time constant (τ) in the presence of varying concentrations of different α Syn species is given. Data are presented as mean \pm SD. The experiment was performed with three α Syn concentrations and $n = 3$ independent replicates per α Syn concentration (independent addition of α Syn to AK2), except for 0.238 μ M of α Syn monomer and 1.2 μ M of α Syn fibrils,

which were tested with $n = 2$ replicates. Asterisk indicates statistically significant difference between given condition and control in the absence of α Syn (p -value = 0.0146, two-tailed t -test). Supplementary Fig. 6 shows an orthogonal assay testing the activity of AK2 influenced by α Syn. **c–g** Light scattering aggregation assay of WT (c), Δ C (d), E46K (e), A53T (f), and A30P (g) α Syn at a concentration of 300 μ M in PBS pH 7.4 in the absence or presence of varying concentrations of AK2. The experiment was performed in triplicate. Mean values and SD are shown. **h** SDS-PAGE of α Syn pellet obtained after incubation of α Syn (300 μ M) in the absence or presence of AK2 at different concentrations (150 μ M, 300 μ M, and 600 μ M). The molar ratios of AK2 to α Syn are given at the top of the gel. The experiment in (h) was repeated twice independently. Source data are provided as a Source Data file.

Next, we wondered if AK2 influences the aggregation rate of α Syn at (sub-)stoichiometric amounts and performed a light scattering (Fig. 4c–g) and Thioflavin T (ThT) kinetic aggregation assay (Supplementary Fig. 7) of α Syn in the presence of varying concentrations of AK2. At steady state, the abundance of WT α Syn fibrils measured by light scattering or ThT fluorescence emission was lower for samples with higher concentrations of AK2 (Fig. 4c and Supplementary Fig. 7). This was confirmed by SDS-PAGE of the pelleted fibrils at the end of the aggregation kinetics in the absence and presence of different AK2 concentrations (Fig. 4h). TEM imaging of the generated fibrils showed visually less fibrils in the presence of AK2 without obvious difference in

fibril topology (Supplementary Fig. 8). These data could be explained by complex formation between AK2 and monomeric α Syn interfering with aggregation. To further explore the potential relevance to PD of an inhibitory effect of AK2 on α Syn, we tested whether AK2 inhibited the aggregation of Δ C- α Syn, as a PTM relevant for PD, and the PD-related familial mutants E46K, A53T, and A30P. In contrast to WT α Syn, AK2 did not considerably influence the aggregation kinetics of Δ C- α Syn (Fig. 4d), and of familial variants E46K and A53T (Fig. 4e, f). For the A30P mutant, some inhibitory effect was observed, however, smaller compared to that observed for WT α Syn (Fig. 4g). Although the mechanism by which familial mutants influence α Syn aggregation

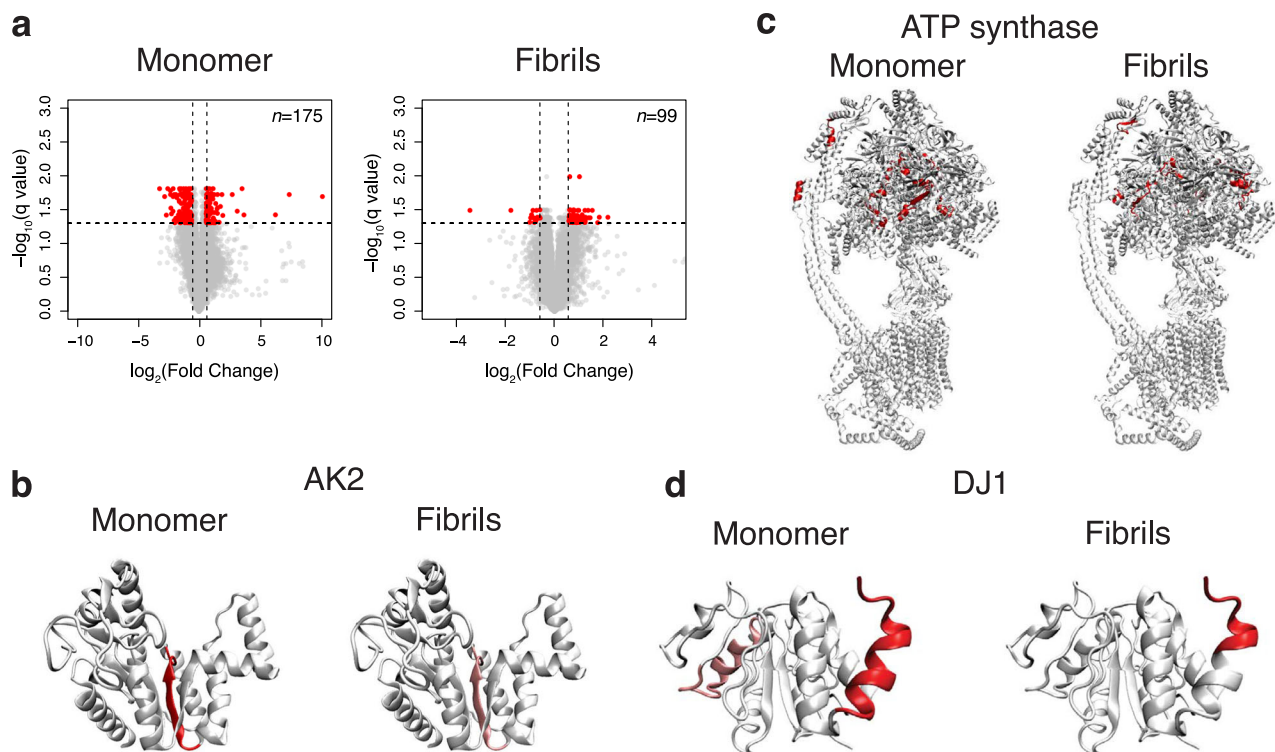


Fig. 5 | α Syn conformation-dependent interaction with AK2, DJ1, and ATP synthase. **a** Volcano plot shows LiP-MS results on peptides significantly changing upon mitochondrial treatment with α Syn fibrils or monomers for 30 min. Red dots show statistically significant hits (Fold Change > 1.5, q -value < 0.05, based on a two-tailed t -test followed by Benjamini–Hochberg adjustment for multiple hypothesis testing). LiP-MS hits peptides mapped to the protein structure when treated with α Syn monomer or fibrils for AK2 (**b**), ATP synthase (**c**), and DJ1 (**d**). The peptide

changes found for AK2 were the same as with α Syn monomers, while for DJ1, only one of two regions found with monomers were also found with α Syn fibrils. Hits passing the q -value cutoff (<0.05) are shown in red. **b, d**, peptides significant only at a p -value cutoff (<0.05) are shown in pink. p -values were calculated using a two-tailed t -test. FDR adjustment was used for q -value determination. Source data are provided as a Source Data file.

kinetics in the presence of AK2 is not obvious, it can be explained by additional interaction sites of AK2 on the N-terminus of α Syn. Furthermore, it appears evident that deletion of the major AK2 binding site in the Δ C- α Syn construct results in a loss of aggregation inhibition by AK2.

α Syn interacts with multiple proteins in intact mitochondria

Next, we wanted to characterize how α Syn interacts with intact mitochondria, to better mimic a physiological scenario. We tested both monomeric and fibrillar α Syn to reveal possible conformation-specific effects. We asked which proteins α Syn can access/interact with within intact mitochondria or which proteins it can affect indirectly via downstream events. We incubated the mitochondrial fraction without lysis with monomeric WT α Syn and with α Syn fibrils for 30 min, a longer incubation than performed with lysed mitochondria. These conditions were used to assess whether α Syn could cross the mitochondrial membrane and access AK2 in the IMS, thereby interacting with it in a more physiological context. In this LiP-MS experiment, we detected 175 candidate interactors of monomeric and 99 candidate interactors of fibrillar α Syn (Fig. 5a and Supplementary Data 1 and 2, respectively). The same peptide of AK2 protein identified in the experiment with lysed mitochondria (94 NGFLLDGFPR 103) was significantly changed in the presence of α Syn monomer (q -value < 0.05, FC > 1.5) and α Syn fibrils (Fig. 5b), although the change in the presence of fibrils was only significant before p -value correction for multiple testing (p -value < 0.05, FC > 1.5). Notably, the C-terminus segment is highly flexible in most of the amyloid fibril polymorphs of α Syn^{54–57}. Multiple ATP synthase subunits were also structurally altered upon addition of both monomeric and fibrillar α Syn (Fig. 5c). In the presence of the monomer, we detected structural changes in subunit β (part of

the F_1 domain), peripheral stalk subunits b and d, and end of membrane subunit e. In the presence of fibrils, we detected structural responses in subunits α , β , and OSCP. We note, however, that in this experimental set-up we cannot exclude the presence of a fraction of non-intact mitochondria caused by destruction of mitochondrial membrane integrity by α Syn fibrils. Furthermore, in this set-up, we cannot distinguish whether these interactions are direct physical interactions or downstream, indirect effects of direct binding events. However, our data suggest that ATP synthase structurally responds to the addition of monomeric and fibrillar α Syn⁴⁶.

DJ1 was also significantly altered in the presence of α Syn (Fig. 5d). Despite not being the strongest hit, DJ1 is of particular interest because mutations in the gene that encodes DJ1 are associated with early-onset PD⁵⁸. DJ1 is a small ubiquitous protein that protects cells from oxidative stress and mitochondrial injury^{59,60}. In cells under oxidative stress, DJ1 translocates into dysfunctional mitochondria to induce autophagy; thus, loss of DJ1 results in the accumulation of faulty mitochondria^{61,62}. Furthermore, DJ1 interferes with the function of α Syn in regulating the fusion and fission of mitochondria¹⁹. The peptides identified for DJ1 in our LiP-MS experiment were the residues 107–121 and 176–189. The peptide 107–121 includes the fourth α -helix (i.e., residues 109–114) and a flexible region (Supplementary Fig. 9). The C-terminal peptide 176–189 includes the ninth α -helix (i.e., residues 175–185), which is exposed at the surface of the protein. Both these regions remain accessible in the functional dimer of DJ1⁶³. The site where DJ1 binds to α Syn was investigated by 2D [15 N, 1 H]-HMQC of 15 N-labeled α Syn in the presence of varying concentrations of DJ1. Major CSPs were observed throughout the protein sequence, with the strongest changes around Met5 at the N-terminus of α Syn and residues 105 to 135 at the C-terminus (with CSP > 0.01 ppm shown in Supplementary Fig. 9b).

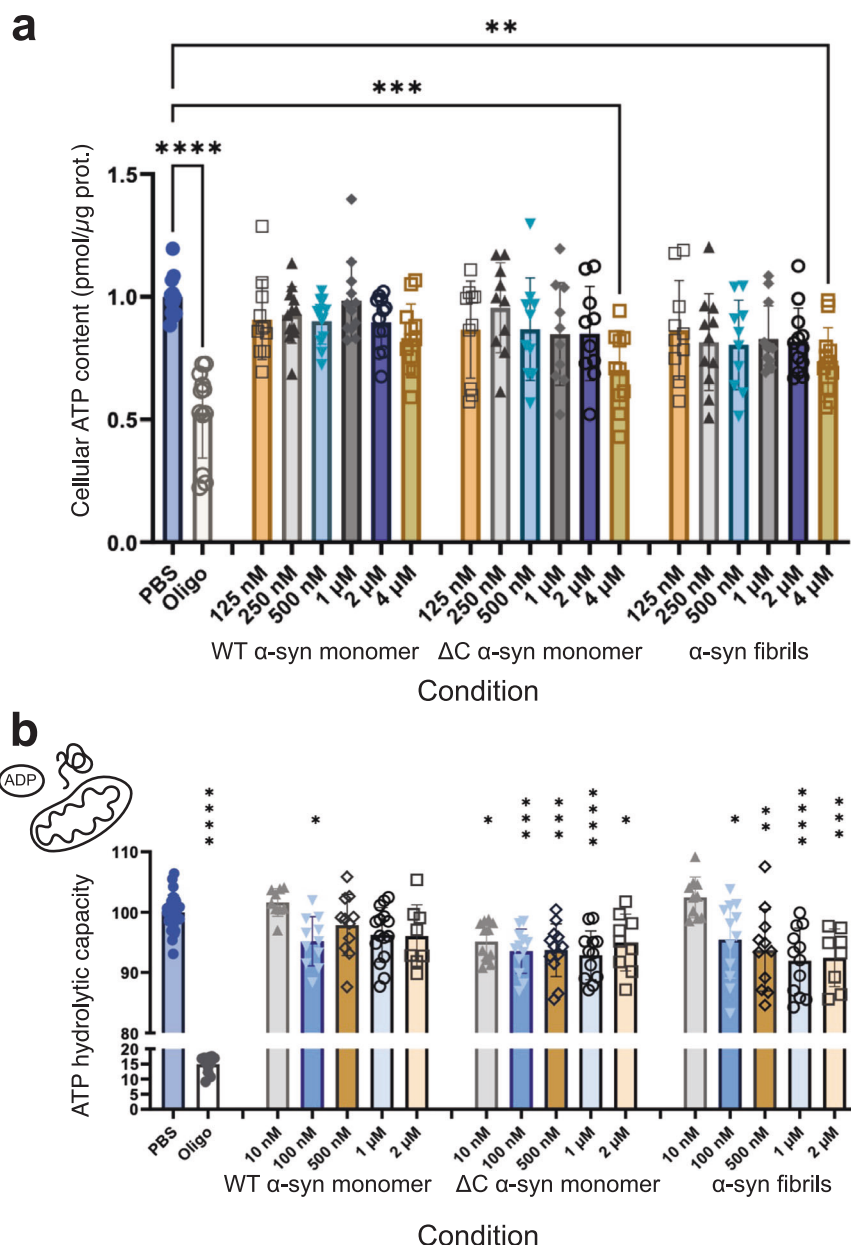


Fig. 6 | Influence of α Syn on ATP hydrolysis in cells. **a** Whole cellular ATP content in mice HT-22 cells in the presence of WT and Δ C- α Syn monomers and fibrils. **b** ATP hydrolytic capacity in isolated mice liver mitochondria after the addition of increasing concentrations of WT and Δ C- α Syn monomers and fibrils. PBS treatment was used as a control, and its hydrolytic activity was set at 100%. Oligomycin A, a potent ATP Synthase inhibitor, was used as a positive control. Statistical significances were calculated with one-way ANOVA followed by Dunnett's multiple

comparisons test. **** p -value < 0.0001, *** p -value < 0.001, ** p -value < 0.01, * p -value < 0.05. p -value \geq 0.05 was considered non-significant. All data are given as mean \pm SD. Experiments for each setup were performed on four separate days (**a**, **b**). In total, $n = 10$ –12 replicates for (**a**) and $n = 8$ –15 replicates for (**b**) were used for each condition. Exact p -values and n for each condition are provided in the Source Data file. Source data are provided as a Source Data file.

These findings indicate that α Syn interacts with DJ1 at multiple interaction sites. When compared with the CSP fingerprint of α Syn in mitochondria, DJ1 binding could account for the CSPs observed from residue 50 onward, which include the NAC region. Similarly, the fingerprint of the peak intensity ratios broadly follows the pattern observed for mitochondria. Hence, DJ1 alters the accessibility of α Syn at regions that include the AK2 binding site in the C-terminus, and this interaction is of transient nature.

As expected from a highly plastic intrinsically disordered protein, LiP-MS experiments indicate that α Syn interacts with multiple mitochondrial proteins. Interestingly, the NMR intensity profile comprising about 100 probes obtained for 15 N-labeled monomeric WT α Syn in the presence of lysed mitochondria can be modeled as a linear

combination of the α Syn spectra in the presence of AK2, DJ1, and cardiolipin (Supplementary Fig. 10). However, additional interaction partners are expected to contribute as an accurate reconstruction requires a 20% contribution from other binders, based on the linear combination approach.

α Syn affects ATP homeostasis in isolated mitochondria and in intact cells

Since we detected multiple mitochondrial proteins related to ATP hydrolysis and ATP homeostasis, including AK2 and ATP synthase, structurally responding to α Syn in our experiments (including direct interactions), we measured ATP content in cells and isolated mitochondria exposed to different concentrations of α Syn species ranging

from 125 nM to 4 μ M. PBS was used as a control, and oligomycin A, a potent ATP synthase inhibitor, was used as a positive control. ATP content in HT-22 cells, immortalized mouse hippocampal cells, decreased after 24 h of incubation with 4 μ M monomeric Δ C- α Syn, in contrast to PBS-treated control cells (Fig. 6a). Lower concentrations did not significantly impact ATP hydrolysis. In contrast, the WT α Syn monomer did not have a significant effect on ATP content at any concentration tested (Fig. 6a). WT α Syn fibrils at 4 μ M concentration showed, however, decreased ATP content. Similarly, both monomeric Δ C- α Syn and WT α Syn fibrils significantly reduced the ATP hydrolytic capacity in isolated liver mitochondria, whereas WT α Syn monomers did not have any effect relative to PBS treatment (Fig. 6b). Notably, α Syn has been found to accumulate in liver and hepatocytes^{64,65}. Like α Syn fibrils, C-terminally truncated α Syn is found in Lewy bodies and is thought to be pathology-associated^{66,67}. Our data suggest that these species inhibit ATP hydrolysis in cells and isolated mitochondria in a similar manner.

Discussion

In this work, the uptake/binding of α Syn into/onto mitochondria up to a concentration of $2 \mu\text{M} \pm 0.5 \mu\text{M}$ was observed. In its intrinsically disordered state, α Syn transiently interacts with both the membrane as well as a subset of soluble mitochondrial proteins, including DJ1 and AK2, activating the latter. Detailed NMR investigations revealed that the membrane interaction site on α Syn is the positively charged N-terminal region, as expected³⁹ while the negatively charged C-terminal segment interacts with both DJ1 and AK2. WT monomeric α Syn has an activating effect on AK2, hinting towards a possible physiological role of α Syn in the energy production of mitochondria. Interestingly, fibrillar α Syn did not have a significant effect on AK2 function. Moreover, light scattering and ThT aggregation assays, together with SDS-PAGE of WT α Syn pellets, show that AK2 modulates α Syn aggregation and increases the percentage of α Syn remaining in the soluble, non-fibrillated form. Interestingly, the effect of AK2 on the aggregation of α Syn was reduced for A30P α Syn and lost for PD-associated α Syn familial mutants E46K and A53T, as well as for the C-terminally truncated α Syn variant, which is a PD-related PTM^{68–70}. Furthermore, the latter did not show a positive impact on AK2 function, and reduced ATP production in cells and isolated mitochondria, resulting in a coherent picture of the relationship between α Syn and ATP homeostasis. In the future, it would be interesting to test the effects of other α Syn PTMs, especially phosphorylation of Ser129, a modification associated with pathology^{66,67,71}. Due to its C-terminal location, pSer129 α Syn might interact differently with AK2. Moreover, investigating the effects of α Syn oligomers in future studies would be of interest.

Furthermore, WT α Syn monomers and fibrils both triggered structural responses in the ATP synthase; however, we detected different structural changes in response to different conformations of α Syn. This interaction could be direct or indirect, e.g., because of the change of adenine nucleotide balance in mitochondria. The possible physiological impact of monomeric α Syn on ATP synthase was shown previously, while oligomeric species reduce ATP synthase activity⁷². Our data complement these earlier findings for the ATP synthase, providing new structural insights on the regions involved in the response of ATP synthase to different α Syn conformations^{45,46}. Furthermore, here, we revealed that AK2, another important player in mitochondrial ATP homeostasis, is functionally regulated by α Syn in a conformation-dependent manner.

Our functional validation on ATP production in intact cells and isolated mitochondria showed that indeed α Syn conformations are associated with pathology, i.e., fibrils and Δ C- α Syn, reduce ATP production in both systems, while the monomeric form does not. However, we also did not observe an enhancement of ATP production for α Syn WT monomers. This lack of enhancement could reflect more

complex regulation of ATP homeostasis with rate-limiting steps controlled by other molecular players.

In our experiments with intact mitochondria under prolonged incubation time, the interaction between α Syn and mitochondrial proteins that are not exposed to the surface (Fig. 5) can be explained by translocation of α Syn into mitochondria for monomeric α Syn, or due to destruction of mitochondrial membrane integrity in the case of α Syn fibrils, or due to indirect effects downstream of the interaction of α Syn with mitochondrial surfaces.

We compared the interactors of α Syn revealed with LiP-MS and the interactors that were identified with the other methods for the α Syn monomer⁷³ and for α Syn upon Lewy Body pathology⁷⁴. Five out of 18 of our LiP-MS hits for α Syn monomer (TPII, GDA, DDX17, SPTN1, and TRIC complex) were also identified as interactors of α Syn in the previous study⁷³. Next, we compared our LiP-MS-based candidate interactors of α Syn fibrils with the interactors of α Syn specific to Lewy pathology identified by the biotinylation by antibody recognition method (BAR). We found a remarkable overlap between our LiP-MS hits and the proteins identified by BAR; specifically, 38 and 67 out of 99 of LiP-MS hits for α Syn fibrils were detected as interactors of pSer129 α Syn and total α Syn in synucleinopathies, respectively, relative to healthy controls. This shows a reassuring correlation between the results obtained with the two techniques and the complementarity of the LiP-MS and BAR approaches. In addition, LiP-MS provided structural information on these Lewy pathology-relevant interactors and pinpointed potential interaction interfaces (Supplementary Data 2). Furthermore, LiP-MS identified 32 new candidate interactors of α Syn fibrils. While ATP synthase and DJ1 were also found interacting with α Syn upon Lewy pathology using BAR, AK2 has not been previously reported to interact with α Syn.

Overall, our results offer a new perspective on the potential physiological role of α Syn monomers in maintaining ATP homeostasis in mitochondria. Whether this is a regular α Syn function or a rescue mechanism under stress when additional ATP is required, remains to be understood. In line with that, PD-associated C-terminally truncated α Syn, familial mutants, and α Syn fibrils did show different effects from monomeric full-length α Syn in multiple functional experiments.

More generally, the data presented show a coherent picture of the potential role of α Syn in ATP homeostasis both at the physiological and pathological levels. It also revealed multiple concomitant interactions of α Syn with mitochondrial proteins. The detection of multiple transient binding sites with cellular material (both proteins and membranes) within the sequence of an IDP with only 140 amino acids highlights the power of IDPs in executing sequence-dense, pluripotent actions of dynamic nature.

Methods

Ethical statement

The animal experiments were carried out in compliance with Swiss Animal Welfare legislation, according to Art.18 Tierschutzgesetz (TSchG), Art. 141 Tierschutzverordnung (TschV), Art. 30 Tierversuchsverordnung (TVV) (all Switzerland), and were approved by the cantonal Veterinary Office of Zurich, Switzerland, under the license 34491 (National Number).

Protein expression and purification

For the recombinant expression of N-terminally acetylated WT α Syn, a pRK172 plasmid containing the *SNCA* gene was cotransformed together with a plasmid encoding for the yeast *N*-acetyltransferase complex B (NatB) into *E. coli* BL21 Star(DE3) cells. The cells were grown and induced in Lysogeny broth (LB) for unlabeled α Syn and M9 minimal media supplemented with ¹⁵NH₄Cl for ¹⁵N-labeled α Syn. The harvested cells were lysed by resuspending them in osmotic shock buffer (Tris buffer with 40% sucrose) and then transferring them to cold ultrapure water. The supernatant after centrifugation was boiled in water for

10 min and cooled down in an ice ethanol bath (-5°C). The crude protein was purified by ammonium sulfate precipitation (first removing the insoluble parts at 35% saturation at room temperature, afterwards αSyn was precipitated at 60% saturation and resuspended in buffer) and afterwards dialyzed into Tris buffer. Subsequently, the protein was further purified by anion exchange chromatography using a HiTrap™ Q FF 16/10 column (from GE Healthcare) equilibrated with Tris buffer. The clean protein was eluted using a gradient from 0% to 50% 1 M NaCl in Tris buffer over 200 ml. The fractions containing αSyn were pooled, dialyzed into pure water, and lyophilized for later usage. Purity was confirmed using SDS page and ^{15}N , ^1H -HMQC NMR. The $\Delta\text{C-}\alpha\text{Syn}$ (i.e., αSyn (1–121)) was expressed and purified in the same way using a plasmid modified by site-directed mutagenesis. We note that N-terminally acetylated human recombinant αSyn was used throughout all experiments, including when non-human material such as bovine mitochondria was used (see below).

AK2 was recombinantly expressed using a pET-42b(+) plasmid. The construct contains an N-terminal histidine tag connected via a TEV-cleaving site. Expression of labeled and unlabeled protein was done like explained for αSyn . The cells were lysed using an ALT M-110S Microfluidizer, and insoluble parts were removed by centrifugation. Firstly, the crude protein was purified by employing two 5 ml HisTrap™ Fast Flow columns equilibrated with a 25 μM imidazole Tris buffer. The protein was eluted using 250 μM imidazole Tris buffer. The fractions containing AK2 were identified by SDS page, pooled, and dialyzed. After concentrating the protein using a 10 kDa spin filter tube, the His-tag was removed by the addition of TEV protease in a ratio of 1:50 and incubation at 4°C overnight. The cleaved tag was removed by another 5 ml HisTrap™ column. The protein was dialyzed into Tris buffer, concentrated, and stored as aliquots at -20°C . Purity was confirmed using SDS page, and activity was confirmed using NMR and luciferase-based ATP assay (ATP Kit SL from BioThema).

Human PARK7(DJ1) was bought from Abcam in lyophilized powder form (ab124312).

The Membrane Scaffold Protein (MSPdH5) used for the formation of nanodiscs was expressed on a pET-28a plasmid. Like AK2, the construct contained an N-terminal His-tag and TEV-cleaving site. Expression and purification were analogous to the purification of AK2.

Skp purification was performed as previously described in ref. 75. Skp was recombinantly expressed using a pET28b plasmid expression vector (Novagen). The construct contains an N-terminal histidine tag connected via a TEV-cleaving site. BL21-(λ DE3)-Lemo cells (New England Biolabs) transformed with the Skp plasmid were grown at 37°C in LB medium containing kanamycin (30 mg/ml) to OD_{600} (optical density at 600 nm) = 0.6, and then the expression was induced by adding 0.4 mM isopropyl- β -D-thiogalactopyranoside (IPTG) at 25°C for 12 h. The harvested cells were resuspended in 20 ml of lysis buffer per liter of culture (20 mM Tris (pH 7.5), 500 mM NaCl, deoxyribonuclease (DNase) (0.01 mg/ml), ribonuclease (RNase) (0.02 mg/ml), and inhibitor cocktail (cOmplete EDTA-free protease inhibitor; Roche)). Cell lysis was performed using a microfluidizer (Microfluidics) for three cycles at 4°C . The supernatant after centrifugation was applied to a HisTrap™ column and eluted with an imidazole gradient. The fractions containing Skp were identified by SDS page, pooled, and dialyzed against buffer (20 mM Tris (pH 7.5) and 500 mM NaCl) overnight to remove the imidazole. Skp was then denatured with 6 M Gdm/HCl, applied to the HisTrap™ column, and eluted with 250 mM imidazole. The eluted Skp was refolded overnight against refolding buffer (25 mM HEPES, pH 7.5, and 150 mM NaCl). The His-tag was removed by the addition of TEV protease in a ratio of 1:100 and incubation at 4°C overnight. The cleaved tag was removed by another 5 ml HisTrap™ column. In a final step, a size exclusion chromatography (Superdex-200 16/600 PG) step was applied to further purify the proteins and adjust the protein to its final buffer (20 mM MES (pH 6.5) and 150 mM NaCl). Purity was confirmed using SDS-PAGE. Afterward, Skp was

concentrated by ultrafiltration and stored at -20°C until use. The final yield of purified protein was 25 mg of Skp per liter of LB medium.

LiP-MS

LiP-MS was performed as described previously in refs. 34,35. Briefly, mitochondrial fraction in LiP buffer (100 mM HEPES pH 7.5, 150 mM KCl, 1 mM MgCl_2) was distributed among technical replicates (four) for each condition. Isolated mitochondrial fraction was incubated with WT αSyn monomer, fibrils, $\Delta\text{C-}\alpha\text{Syn}$, or buffer (for control) for a defined period (15 min or 30 min). PK was added to all samples for 5 min at a 1:100 enzyme-to-substrate ratio, and samples were incubated at 25°C for 5 min. PK digestion was stopped via heat inactivation at 99°C for 5 min, followed by incubation of the samples for 5 min on ice. An equal volume of sodium deoxycholate was added to a final concentration of 5% (w/v). Next, TCEP was added to a final concentration of 5 mM and incubated at 37°C for 30 min in a thermomixer under shaking (800 rpm). For alkylation of reduced cysteines, iodoacetamide was added to a final concentration of 40 mM and samples were incubated for 30 min in the dark. To dilute sodium deoxycholate to the final concentration of 1%, we used 0.1 M ammonium bicarbonate. The samples were digested for 16 h at 37°C by LysC and trypsin at a 1:100 enzyme/substrate ratio. Digestion was stopped by lowering the pH with formic acid. The samples were centrifuged, and supernatants were desalted on Sep-Pak tC18 cartridges (Waters). Samples were eluted with 80% acetonitrile, 0.1% formic acid.

AP-MS

A SH-SY5Y cell pellet was lysed in IP buffer (LiP buffer + 1 \times complete protease inhibitor, 1 \times PhosSTOP). The lysate was split into the requisite number of aliquots prior to spiking in αSyn (5 μg) and rotated 1 h at room temperature (end-to-end rotation). αSyn was immunoprecipitated with anti- αSyn antibody (abcam MJFR1, ab13,8501, 4 μg) for 2 h at 20°C under constant end-to-end rotation using protein A conjugated magnetic beads. As a negative control, an isotype-specific Ig control was used with magnetic protein A beads. Four replicates were used for each condition. Beads were collected on a DynaMag-2 magnetic rack, washed 6 \times with LiP buffer. The proteins were eluted in 60 μl 8 M urea for 30 min at 37°C (1500 rpm, Eppendorf shaker) and snap-frozen. The classical trypsin digestion workflow was applied (see LiP-MS section).

Acquisition of LC-MS/MS data and data analysis

LC-MS analysis was carried out on the Orbitrap Q Exactive Plus or Orbitrap Fusion Lumos Tribrid mass spectrometer (Thermo Fisher Scientific) equipped with a nano-flow LC system (Easy-nLC1200, Thermo Fisher Scientific) and custom-packed columns with 1.9 μm C18 beads. The separation protocol used a linear gradient of acetonitrile in buffer (water and 0.1%FA) increasing from 5% to 35% over 120 min.

DIA scans were conducted in 20 or 41 variable-width windows. MS1 scans covered a mass range of 350–1400 m/z with a resolution set at 120,000 with a maximal injection time of 100 ms. HCD was used for fragmenting precursor ions. DIA-MS/MS spectra were captured using an Orbitrap with a resolution of 30,000 and a scan range of 350–1150 m/z , with a maximal injection time set to 54 ms.

Raw DIA LC-MS/MS data were searched using Spectronaut 17 (Biognosys AG) with default settings, except that semi-specific digestion was selected. Mass tolerances were defined during data analysis in Spectronaut using default (dynamic) mass tolerance settings. The number of missed cleavages was set to two, and the minimum peptide length was set to seven amino acids. The following fixed modification was applied: carbamidomethyl (C). Variable modifications included acetylation at the protein N-terminus and oxidation of methionine (M). The FASTA file used for the search of the bovine proteome was UP000009136. Library samples were acquired in DDA mode. The data were analyzed in R using the limma, dplyr, tidyr, and ggplot2 packages. Median normalization was performed prior to testing for differential

abundance at the peptide level. Both half-tryptic and fully tryptic peptides were included in the analysis. *p*-values were calculated using a two-tailed, unpaired Welch's *t*-test. The Benjamini–Hochberg method was applied to adjust for multiple hypothesis testing and to calculate FDR-adjusted *p*-values (*q*-values). The visual molecular dynamics (VMD) software was used to visualize protein structures.

αSyn fibril production

All mature αSyn fibrils used were formed from a starting solution of 500 μM unlabeled WT αSyn in PBS buffer at pH 7.4 + 0.02% NaN₃. Five hundred microliters of the starting solution in a 0.5 ml Eppendorf tube was incubated at 37 °C on a rotating mixer spinning at 30 rpm for more than two weeks. Before usage, the formed fibrils were pelleted by centrifugation and washed three times with PBS buffer.

ThT aggregation study

Samples were prepared to contain 500 μl of 300 μM αSyn in PBS pH 7.4 and varying concentrations between 0 μM and 240 μM AK2 in a 0.5 ml Eppendorf tube. All tubes were incubated at 37 °C on a rotating mixer spinning at 30 rpm for a total of 145 h. To acquire a time point, 5 μl of sample was diluted into 200 μl PBS buffer and 2 μl 1 mM ThT. The data was recorded on a Horiba-Jobin Yvon (FluoroMax 4) spectrofluorometer using an excitation wavelength of 450 nm and collecting emission in the range 465–500 nm with a slit width of 5 nm. For analysis of the data and sigmoidal fitting, Matlab version R2019a has been used.

Pull down experiment 1D

A tube containing 300 mg of bovine mitochondria was washed two times with 800 μl PBS and later resuspended in 60 μl PBS. Roughly 2 mg of lyophilized WT αSyn was dissolved in 500 μl PBS buffer and added to the mitochondria. The mixture was incubated at room temperature for 15 min. Afterwards, the mixture was put into 25 ml of PBS with 4% D₂O. The mitochondria were recovered by centrifugation, and this washing step was repeated two more times. The mitochondria pellet was transferred to a 5 mm Shigemi tube and immediately measured by NMR. The supernatant of the last washing step was used as a control.

Nanodisc preparation

To start with, a stock solution (>200 μM) of MSPdH5 in 20 mM Tris with 200 mM sodium chloride was prepared, as well as a 50 mM stock of cardiolipin (18:1) in 200 mM sodium cholate. The stocks were mixed to get 1 ml of a 5 mM cardiolipin, 200 μM MSPdH5 (25:1) solution, which was incubated and mixed at room temperature overnight. 1 g of bio beads was added in small portions over the course of 6 h to extract excessive lipids. After removing the beads by centrifugation, the formed nanodiscs were isolated using a Superdex 200 10/300 column (GE Healthcare) for size exclusion. All fractions were examined using Interferometric Scattering Mass Spectrometry (ISCAMS). All fractions where the expected mass of 128 kDa was found as the only major component were combined and stored at 4 °C.

Extraction of the bovine brain mitochondria-enriched fraction

All the material (scalpel, scissors, homogenizer, dishes, and spatula) and buffers were precooled to 4 °C. The whole procedure was performed on ice, and all instruments (centrifuges) were cooled down to 4 °C. The extraction buffer used contained 125 mM sucrose, 125 mM Mannitol, 10 mM HEPES, 7 mM EGTA, 0.01% bovine serum albumin, and four tablets of protease inhibitor cocktail per 1.5 l of buffer. A fresh bovine brain was purchased from the “Veterinärdienst Stadt Zürich” and arrived in the lab around 26 h after extraction. The brain was washed with cold extraction buffer to remove the blood. From an initial weight of around 500 g, around 200 g of white matter was extracted using a scalpel, scissors, and spoons. The white matter

pieces were washed three times and minced as small as possible using scissors. Four milliliters of extraction buffer per gram of white matter were added. The tissue was homogenized using a glass tissue grinder. Around 15 to 20 strokes were used per portion. The mixture was centrifuged at 1000× *g* for 30 min, followed by a 10,000× *g* centrifugation for the supernatant. The pellet of the second step was washed three times with PBS buffer pH 7.4 with 1% bovine serum albumin and afterwards dissolved in the same buffer with 10% DMSO, aliquoted, and stored at –80 °C. Whenever mitochondria were used for experiments, a tube was thawed and washed three times with the desired buffer to remove the DMSO. When lysed mitochondria were used, freeze–thaw cycles together with ultrasonication were employed. Functionality of the intact mitochondria was assessed using a luciferase-based bioluminescence assay (Supplementary Fig. 1).

Luciferase-based ATP bioluminescence assay

The assay was performed using the ATP Kit SL from BioThema. The light was detected using a PherAstar Plus plate reader with a luminescence module installed. All samples had a final volume of 200 μl. All samples contained 25 μM NAD⁺, 25 μM ADP in 100 mM Tris pH 7.5, and around 1–2 mg of a bovine brain mitochondria pellet. To some wells, 500 μM pyruvate and 500 μM malate were added, to others 5 mM Glutamate and 500 μM malate. Blanks contained all the metabolites but no mitochondria. All the relevant metabolites and the mitochondria were prepared to be 160 μl in a well of a Greiner F-Bottom 96 plate. The reaction was initiated using 40 μl of the SL buffer containing luciferase. Acquired were 200 points with an acquisition time of 1 s over the course of 1 h.

NMR sample preparation

All in vitro samples were prepared using phosphate buffer saline (PBS). αSyn, ΔC-αSyn, and AK2 were added from stock solutions. To remove oligomeric species, αSyn and ΔC-αSyn stocks were filtered with a 100-kDa molecular weight cut-off concentrator (Amicon) before being used for NMR sample preparation. To ensure that the AK2 stock only contained monomeric protein, the thawed protein was reduced using TCEP (tris(2-carboxyethyl)phosphine), and monomeric AK2 was isolated by size exclusion with a HiLoad™ 26/60 Superdex 75 column (GE Healthcare). The concentrations were determined photometrically by measuring the absorbance at 280 nm with the molar absorption coefficients $\epsilon = 5960 \text{ M}^{-1} \text{ cm}^{-1}$ for αSyn, $\epsilon = 1490 \text{ M}^{-1} \text{ cm}^{-1}$ for ΔC-αSyn, and $\epsilon = 7700 \text{ M}^{-1} \text{ cm}^{-1}$ for AK2. After the addition of the proteins and other components, the pH was adjusted to the desired value using diluted HCl/NaOH solutions. Each sample was supplemented with 5% D₂O and adjusted to a final volume of 400 μl in a 5-mm (diameter) Shigemi tube. The samples were measured immediately after preparation.

2D NMR measurement parameters

All 2D NMR experiments were performed on a Bruker 600 MHz Avance III HD spectrometer with a cryogenic proton-optimized ¹H{¹³C/¹⁵N} TCI probe. The pulse sequence employed was a 2D [¹⁵N,¹H] SOFAST HMQC NMR experiment. For the 150 μM sample of ¹⁵N-labeled AK2, the following parameters were used: 256 × 2048 complex points, 128 scans, 1 s interscan delay, and a spectral width of 13.7 ppm for ¹H and 36 ppm for ¹⁵N at 25 °C. For the ¹⁵N labeled αSyn samples with DJ1, the sample contained 30 μM αSyn and 0 μM, 15 μM, 30 μM, or 60 μM DJ1. The following parameters were used: 256 × 2048 complex points, 256 scans, 0.5 s interscan delay, and a spectral width of 11 ppm for ¹H and 30 ppm for ¹⁵N at 10 °C. For the ¹⁵N-labeled αSyn samples with mitochondria, the sample contained 20 μM αSyn and 50 mg lysed mitochondria. The following parameters were used: 128 × 2048 complex points, 512 scans, 0.1 s interscan delay, and a spectral width of 14 ppm for ¹H and 31 ppm for ¹⁵N at 10 °C. For the ¹⁵N-labeled αSyn samples with cardiolipin nanodiscs, the sample contained 20 μM αSyn

and 20 μM nanodiscs. The following parameters were used: 256×2048 complex points, 64 scans, 0.5 s interscan delay, and a spectral width of 12 ppm for ^1H and 30 ppm for ^{15}N at 10°C . For the ^{15}N -labeled αSyn samples with AK2, the sample contained 20 μM αSyn and 110 μM AK2. The following parameters were used: 128×2048 complex points, 128 scans, 0.5 s interscan delay, and a spectral width of 11 ppm for ^1H and 30 ppm for ^{15}N at 10°C . All NMR spectra were processed with TopSpin 4. Visualization and data analysis were carried out in SPARKY. Peak intensities and chemical shift differences extracted from SPARKY were further analyzed using LibreOffice Calc. The pH in the NMR experiments was controlled further by the chemical shift of His50 (Supplementary Fig. 11).

AK2 activity assay by NMR

The experiments were performed on a Bruker 700 MHz Avance III spectrometer with a cryogenic proton-optimized $\{^1\text{H}\{^{13}\text{C}\}^{15}\text{N}\}$ TCI 700 probe. A 60 μM AK2 solution was prepared in Tris buffer with 150 mM NaCl, 5% glycerol, and 0.1 mM DTT. The starting solution contained 1 mM DSS, 10 mM 98% D Tris, 2 mM ATP, 1 mM AMP, and 10% D_2O in a final volume of 630 μl in a 5 mm NMR tube. Depending on the sample, the starting solution contained either 238 nM, 1.2 μM , or 4.8 μM of αSyn , $\Delta\text{C-}\alpha\text{Syn}$, or αSyn fibrils. Triplicates of all conditions were recorded. The experiment was set up using the starting solution. Afterwards, the tube was briefly removed from the spectrometer to initiate the reaction using 5 μl AK2 stock (238 nM final AK2 concentration). A pseudo 2D experiment was recorded, consisting of 200 proton 1D spectra with 16384 complex points, 16 scans, a delay time of 0.3 s, and a spectral width of 16 ppm at 25°C . The peaks of the H8 adenine protons of ATP, ADP, and AMP were integrated in Topspin 4. The values were fitted with an exponential function in MATLAB R2019a.

AK2 activity assay by UV/VIS spectroscopy

The UV/VIS spectroscopy approach used here is based on the method described by Song et al.⁵². A 60 μM AK2 solution was prepared in Tris buffer with 150 mM NaCl, 5% glycerol, and 0.1 mM DTT. The starting solution contained 2 mM ATP, 0.6 mM AMP, 93 μM bromothymol blue, 0.1 mM glycine-NaOH, and 5 mM magnesium acetate. Depending on the sample, the starting solution included 1.2 μM , 4 μM , or 6 μM of αSyn , $\Delta\text{C-}\alpha\text{Syn}$, or αSyn fibrils. The reaction was initiated using 10 μl of the AK2 stock added to 1.5 ml starting solution (final AK2 concentration is 0.4 μM) in a quartz cuvette. The data was recorded on a Jasco V-650 UV/VIS spectrometer at 617 nm at 25°C with a sampling rate of two points per second.

Whole-cell ATP content assay

HT-22 (SCC129, Merck) is an immortalized mouse hippocampal cell line subcloned from the HT-4 cell line⁷⁶. The cells were cultivated and grown in high-glucose DMEM (Sigma, D6429), supplemented with 10% fetal bovine serum (FBS) (ThermoFisher, 10270106) and 1 \times Penicillin-Streptomycin (ThermoFisher, 15140122).

The cellular ATP content in whole cells was determined according to the procedure of Beuster et al.⁷⁷ using the CellTiter-Glo[®] Luminescent Cell Viability Assay (G7571, Promega, Wisconsin, USA). HT-22 cells were plated into a 96-well, clear bottom white microplate (655098, Greiner bio-one, St. Gallen, Switzerland) at a density of 4.5×10^3 cells/well in 100 μl DMEM cell culture medium (cell plate) and allowed to attach overnight at 37°C under 5% CO_2 . Test compounds were added after 24 h, and PBS (<0.1%, Gibco[™] 10010023) and Oligomycin A (5 μM , Adipogen, San Diego, USA) were included as controls. HT22 cells were incubated for 24 h with three different types of $\alpha\text{-Syn}$ (monomers, C-truncated monomers ($\Delta\text{C-}\alpha\text{Syn}$), and fibrils) at increasing concentrations starting from 125 nM until 4 μM for all three types. Fifty microliters per well of triplicate ATP (497354, abcr GmbH) standards in PBS (0 μM , 1 μM , 2 μM , 3 μM , 5 μM , 10 μM ,

and 15 μM) were added to a clear bottom white 96-well plate (ATP standard plate), and 25 μl of Cell titer-Glo buffer was added to each standard well. The ATP standard plate was shaken for 15 min on a horizontal shaker. In the meantime, following the $\alpha\text{-Syn}$ treatment, the test plate was washed with 100 μl PBS, followed by the addition of 50 μl PBS in each well. 25 μl of Cell Titer-Glo buffer was added, and the test plate was shaken for 15 min to lyse the cells. Ten microliters per well aliquots were pipetted from the ATP standard plate and from the test plate into a clear 96-well tissue culture test plate (Protein plate; TPP, Trasadingen, Switzerland) for protein content determination. The final 5 ml of Cell Titer-Glo buffer was combined with the Cell Titer-Glo substrate in the dark and vortexed for a few seconds. Twenty-five microliters of 2 \times cell titer-Glo reagents were added per well to the ATP standard plate and the test plate, and both were incubated for 30 min in the dark with shaking. Luminescence at 530/25 nm was measured using a microplate reader (Synergy HT, BioTek Instruments GmbH, Sursee, Switzerland) exactly after 30 min incubation. A BCA protein determination assay (Pierce[™] BCA Protein Assay Kit, Thermo Scientific, Massachusetts, USA) was performed using the protein plate to calculate the protein concentration per well. Cellular ATP content was calculated by an ATP standard curve and normalized to cellular protein content/well.

Data analysis was performed using Prism Software (Graphpad, version 9.4.1). One-way ANOVA was conducted, followed by Dunnett's multiple comparisons test to determine statistical significance between PBS control and test compounds in the in vitro evaluation.

Isolation of functional mouse liver mitochondria

The mitochondrial isolation process relies on physical properties like size and density, which are not affected by sex. In healthy adult mice, liver mitochondrial yield and integrity are comparable between sexes. Thus, sex is not a critical variable for standard mitochondrial isolation. The studies were carried out on male C57BL/6Ncrl mice (*Mus musculus*, Charles River). The animals were housed in a specific pathogen-free environment at 23°C with a 12 h/12 h light/dark cycle and 48% humidity with ad libitum access to water and food.

The procedure to isolate functional liver mitochondria was adapted from Frezza et al.⁷⁸. A 5-month-old male C57BL/6N mouse (Charles River) ($n=4$) was anesthetized with isoflurane in oxygen/air (1:1), and the absence of pedal reflex was confirmed by forceps to guarantee deep anesthesia before decapitation. The isolation buffer (100 ml) was prepared by the addition of 5 ml of 0.2 M Tris-MOPS, 1 ml of 0.1 M EGTA/Tris, 20 ml of 1 M sucrose, and 74 ml distilled water.

The liver was dissected using a pre-cooled scalpel (4°C). The liver was washed three times in ice-cold isolation buffer and minced into small pieces in a Petri dish on ice. The isolation buffer was discarded, and the pieces were transferred to an on-ice pre-cooled 15 ml homogenizer (B. Braun Biotech International, Potter S), filled with isolation buffer to approximately 10 ml and homogenized by slowly stroking the glass potter rod up and down five times (1200 rpm). The homogenate was centrifuged at $600 \times g$ for 10 min at 4°C , the supernatant was collected and subsequently centrifuged at $7000 \times g$ for 10 min at 4°C . The pellet was subjected to another round of homogenization and centrifugation as previously described. The supernatant was discarded, and the pellet was carefully detached using a brush and a small volume (around 200 μl) of isolation buffer. Finally, the suspension was centrifuged at $7000 \times g$ for 10 min at 4°C , the supernatant was discarded, and the pellet was carefully detached without using additional isolation buffer. The protein concentration was determined with a BCA assay (Pierce[™], Cat No.: 23225), and the isolated liver mitochondria were stored in aliquots at -80°C .

ATP hydrolysis assay in isolated mitochondria

Experimental procedure from the Complex V Activity Assay Kit (Cayman Chemical, Cat No.: 701000) served as the initial basis for the

development of this assay. Experiment was further modified with procedure steps from A. Barrientos⁷⁹, ATP Synthase Specific Activity Microplate Assay Kit (Abcam, Cat No.: ab109716), Haraux et al.⁸⁰, and Fernandez-del-Rio et al.⁸¹. The following solutions were prepared, the pH was adjusted using KOH, and stored in aliquots at -20°C . An assay buffer containing 25 mM HEPES (Fisher BioReagents, Cat No.: BP310-500), 25 mM KCl (Sigma-Aldrich, Cat No.: 60130), and 2 mM hexahydrate MgCl_2 (Sigma-Aldrich, Cat No.: 63068-250 G) in nanopure water with a pH adjusted to 7.8. A 1 M tris-HCl (Sigma-Aldrich, Cat No.: T3253-500G) buffer in nanopure water with a pH of 8.1, a 200 mM KCl, and a 1 M MgCl_2 anhydrous (abcr, Cat No.: AB202972) solution both in nanopure water. On experiment day, the assay and tris-HCl buffer were thawed at RT. Ten mM ATP (abcr, Cat No.: AB497354) and 40 mM PEP monopotassium (BioChemika, Cat No.: 79415) aliquots were prepared in Tris buffer and 12 mM NADH (Sigma-Aldrich, Cat No.: N4505-500MG) in nanopure water and kept on ice. An aliquot of liver mitochondria was diluted to a concentration of 5 mg/ml with the assay buffer and frozen in liquid nitrogen for 3 min and thawed in a thermomixer (Eppendorf, Thermomixer 5436) at 37°C . This procedure was performed four times in total. The mitochondrial suspension was further diluted to a concentration of 1.32 mg/ml with assay buffer and kept on ice. The reaction mix was prepared on ice and contained 2.84 mM KCl, 1.42 mM MgCl_2 , 1.42 U/ml PK (BioChemika, Cat No.: 83328), 1.95 U/ml LDH (Sigma-Aldrich, Cat No.: L1254-SKU), 0.85 μM FCCP (Fluorochem, Cat No.: M04086), 0.26 μM antimycin A (Sigma-Aldrich, Cat No.: A8674-25MG), 1.13 mM PEP, and 638.12 μM NADH in nanopure water. α -Syn samples were diluted to the desired concentration in PBS. In each well of a transparent 96-well tissue culture test plate (TPP®, Cat No.: 92096), 85 μl reaction mix and 25 μl mitochondria suspension in assay buffer were distributed. One microliter of diluted α -Syn samples was added in triplicate, and the reaction was started by adding 2 μl ATP to each well. Immediately, the plate was placed into a preheated microplate reader (Agilent, BioTek Synergy HT), shaken for 2 s, and the absorbance was monitored at 340 nm for 30 min at 37°C .

α Syn aggregation kinetics monitored by light scattering

The aggregation kinetics of WT α Syn and its disease-associated mutants in the presence and absence of AK2 were monitored using a light scattering assay in a 96-well plate. Light molecular weight (LMW) α Syn was prepared using a 100 kDa cutoff filter, and its concentration was adjusted to 300 μM . LMW α Syn was incubated in the presence of AK2 at molar ratios of 1:0.5, 1:1, and 1:2, respectively. The reaction mixture was then transferred to a 96-well plate. Aggregation kinetics were carried out at 37°C and monitored by light scattering, using both excitation and emission wavelengths at 340 nm. The plate was agitated for 5 min before each reading. For each sample, three independent wells were used. To minimize evaporation during the measurements, the plate was properly covered and sealed in the fluorometer at the correct position.

Bis-Tris Gel image with instant blue staining

WT monomeric α Syn was incubated in the presence and absence of different molar ratios of AK2 and allowed to incubate for 5 days at 37°C with slight agitation (50 rpm). The formed fibrils were centrifuged, and the supernatant was discarded. The fibrils were washed three times with PB buffer and centrifuged again. The resulting fibrils were resuspended in gel loading dye containing SDS and 8 M urea and heated at 95°C for 10 min using a dry bath. Ten microlitres from each sample were loaded onto a 4–12% Bis-Tris gel, which was run and then stained with Instant Blue. During heating at 95°C in the presence of SDS and urea, a big fraction of fibrils was converted to monomers. The bands observed around 15 kDa were compared, revealing that in the presence of a higher concentration of AK2, a lower amount of fibrils

formed, as indicated by the less intense monomeric α Syn band at 15 kDa, the same observation was made for non-monomerized species (at higher molecular weights).

AlphaFold predictions

AlphaFold predictions were generated using AlphaFold version 2.3.1 provided by the ETH Scientific IT Services (https://gitlab.ethz.ch/sis/alphafold_on_euler/). The input sequences used were the full-length, unmodified, canonical human sequences of adenylate kinase 2 (AK2; P54819) and α -Syn (P37840).

The pLDDT score overlaid from two viewing angles, as well as the PAE scores, are provided in the Supplementary Figs. 4 and 5, respectively.

Reporting summary

Further information on research design is available in the Nature Portfolio Reporting Summary linked to this article.

Data availability

The mass spectrometry structural proteomics data generated in this study have been deposited in the ProteomeXchange Consortium database via the PRIDE⁸² under accession code **PXD063500**. The raw NMR data are available from the corresponding authors upon request. All data supporting the results of this study can be found in the article, Supplementary Information, and Source Data files. Source data are provided with this paper.

Code availability

The code is available at <https://github.com/tserdiuk666/mitoalphasyn>.

References

- de Rijk, M. C. et al. A population perspective on diagnostic criteria for Parkinson's disease. *Neurology* **48**, 1277–1281 (1997).
- Balestrino, R. & Schapira, A. H. V. Parkinson disease. *Eur. J. Neurol.* **27**, 27–42 (2020).
- von Campenhausen, S. et al. Prevalence and incidence of Parkinson's disease in Europe. *Eur. Neuropsychopharmacol.* **15**, 473–490 (2005).
- McCann, H., Stevens, C. H., Cartwright, H. & Halliday, G. M. Alpha-synucleinopathy phenotypes. *Parkinsonism Relat. Disord.* **20**, S62–67 (2014).
- Theillet, F. X. et al. Structural disorder of monomeric alpha-synuclein persists in mammalian cells. *Nature* **530**, 45–50 (2016).
- Ibanez, P. et al. Causal relation between alpha-synuclein gene duplication and familial Parkinson's disease. *Lancet* **364**, 1169–1171 (2004).
- Meade, R. M., Fairlie, D. P. & Mason, J. M. Alpha-synuclein structure and Parkinson's disease—lessons and emerging principles. *Mol. Neurodegener.* **14**, 29 (2019).
- Davidson, W. S., Jonas, A., Clayton, D. F. & George, J. M. Stabilization of alpha-synuclein secondary structure upon binding to synthetic membranes. *J. Biol. Chem.* **273**, 9443–9449 (1998).
- Nakamura, K. et al. Optical reporters for the conformation of alpha-synuclein reveal a specific interaction with mitochondria. *J. Neurosci.* **28**, 12305–12317 (2008).
- Ghio, S., Kamp, F., Cauchi, R., Giese, A. & Vassallo, N. Interaction of alpha-synuclein with biomembranes in Parkinson's disease—role of cardiolipin. *Prog. Lipid Res.* **61**, 73–82 (2016).
- Huang, M. et al. Impact of environmental risk factors on mitochondrial dysfunction, neuroinflammation, protein misfolding, and oxidative stress in the etiopathogenesis of Parkinson's disease. *Int. J. Mol. Sci.* <https://doi.org/10.3390/ijms231810808> (2022).
- Smolders, S. & Van Broeckhoven, C. Genetic perspective on the synergistic connection between vesicular transport, lysosomal and

- mitochondrial pathways associated with Parkinson's disease pathogenesis. *Acta Neuropathol. Commun.* **8**, 63 (2020).
13. Kann, O. & Kovacs, R. Mitochondria and neuronal activity. *Am. J. Physiol. Cell Physiol.* **292**, C641–657 (2007).
 14. Lin, M. T. & Beal, M. F. Mitochondrial dysfunction and oxidative stress in neurodegenerative diseases. *Nature* **443**, 787–795 (2006).
 15. Faris, R., Moore, R. A., Ward, A., Sturdevant, D. E., & Priola, S. A. Mitochondrial respiration is impaired during late-stage hamster prion infection. *J. Virol.* <https://doi.org/10.1128/JVI.00524-17> (2017).
 16. Shi, X., Zhao, M., Fu, C. & Fu, A. Intravenous administration of mitochondria for treating experimental Parkinson's disease. *Mitochondrion* **34**, 91–100 (2017).
 17. Zambrano, K. et al. Fighting Parkinson's disease: the return of the mitochondria. *Mitochondrion* **64**, 34–44 (2022).
 18. Valdinocci, D. et al. Intracellular and intercellular mitochondrial dynamics in Parkinson's Disease. *Front Neurosci.* **13**, 930 (2019).
 19. Kamp, F. et al. Inhibition of mitochondrial fusion by alpha-synuclein is rescued by PINK1, Parkin and DJ-1. *EMBO J.* **29**, 3571–3589 (2010).
 20. Pozo Devoto, V. M. & Falzone, T. L. Mitochondrial dynamics in Parkinson's disease: A role for alpha-synuclein?. *Dis. Model Mech.* **10**, 1075–1087 (2017).
 21. Pozo Devoto, V. M. et al. alphaSynuclein control of mitochondrial homeostasis in human-derived neurons is disrupted by mutations associated with Parkinson's disease. *Sci. Rep.* **7**, 5042 (2017).
 22. Vicario, M. et al. A split-GFP tool reveals differences in the sub-mitochondrial distribution of wt and mutant alpha-synuclein. *Cell Death Dis.* **10**, 857 (2019).
 23. Martin, L. J., Semenkow, S., Hanaford, A. & Wong, M. Mitochondrial permeability transition pore regulates Parkinson's disease development in mutant alpha-synuclein transgenic mice. *Neurobiol. Aging* **35**, 1132–1152 (2014).
 24. Rostovtseva, T. K. et al. Alpha-synuclein shows high affinity interaction with voltage-dependent anion channel, suggesting mechanisms of mitochondrial regulation and toxicity in Parkinson disease. *J. Biol. Chem.* **290**, 18467–18477 (2015).
 25. Bender, A. et al. TOM40 mediates mitochondrial dysfunction induced by alpha-synuclein accumulation in Parkinson's disease. *PLoS One* **8**, e62277 (2013).
 26. Devi, L., Raghavendran, V., Prabhu, B. M., Avadhani, N. G. & Anandatheerthavarada, H. K. Mitochondrial import and accumulation of alpha-synuclein impair complex I in human dopaminergic neuronal cultures and Parkinson disease brain. *J. Biol. Chem.* **283**, 9089–9100 (2008).
 27. Di Maio, R. et al. Alpha-synuclein binds to TOM20 and inhibits mitochondrial protein import in Parkinson's disease. *Sci. Transl. Med.* **8**, 342ra378 (2016).
 28. Robotta, M. et al. Alpha-synuclein binds to the inner membrane of mitochondria in an alpha-helical conformation. *Chembiochem* **15**, 2499–2502 (2014).
 29. Shavali, S., Brown-Borg, H. M., Ebadi, M. & Porter, J. Mitochondrial localization of alpha-synuclein protein in alpha-synuclein over-expressing cells. *Neurosci. Lett.* **439**, 125–128 (2008).
 30. Shahmoradian, S. H. et al. Lewy pathology in Parkinson's disease consists of crowded organelles and lipid membranes. *Nat. Neurosci.* **22**, 1099–1109 (2019).
 31. Burmann, B. M. et al. Regulation of alpha-synuclein by chaperones in mammalian cells. *Nature* **577**, 127–132 (2020).
 32. Cole, N. B., Dieuliis, D., Leo, P., Mitchell, D. C. & Nussbaum, R. L. Mitochondrial translocation of alpha-synuclein is promoted by intracellular acidification. *Exp. Cell Res.* **314**, 2076–2089 (2008).
 33. Grunewald, A., Kumar, K. R. & Sue, C. M. New insights into the complex role of mitochondria in Parkinson's disease. *Prog. Neurobiol.* **177**, 73–93 (2019).
 34. Cappelletti, V. et al. Dynamic 3D proteomes reveal protein functional alterations at high resolution in situ. *Cell* **184**, 545–559 e522 (2021).
 35. Feng, Y. et al. Global analysis of protein structural changes in complex proteomes. *Nat. Biotechnol.* **32**, 1036–1044 (2014).
 36. Burke, R. E. & O'Malley, K. Axon degeneration in Parkinson's disease. *Exp. Neurol.* **246**, 72–83 (2013).
 37. Murphy, A. N. & Allison, W. S. Mitochondrial function, part B: mitochondrial protein kinases, protein phosphatases and mitochondrial diseases. *Methods Enzymol.* **457**, xxv–xxvi (2009).
 38. Daum, G. & Vance, J. E. Import of lipids into mitochondria. *Prog. Lipid Res.* **36**, 103–130 (1997).
 39. Bartels, T. et al. The N-terminus of the intrinsically disordered protein alpha-synuclein triggers membrane binding and helix folding. *Biophys. J.* **99**, 2116–2124 (2010).
 40. Giasson, B. I., Murray, I. V., Trojanowski, J. Q. & Lee, V. M. A hydrophobic stretch of 12 amino acid residues in the middle of alpha-synuclein is essential for filament assembly. *J. Biol. Chem.* **276**, 2380–2386 (2001).
 41. Piazza, I. et al. A map of protein-metabolite interactions reveals principles of chemical communication. *Cell* **172**, 358–372 e323 (2018).
 42. Holfeld, A. et al. Systematic identification of structure-specific protein-protein interactions. *Mol. Syst. Biol.* **20**, 651–675 (2024).
 43. Dzeja, P. & Terzic, A. Adenylate kinase and AMP signaling networks: metabolic monitoring, signal communication and body energy sensing. *Int. J. Mol. Sci.* **10**, 1729–1772 (2009).
 44. Noma, T. Dynamics of nucleotide metabolism as a supporter of life phenomena. *J. Med. Invest.* **52**, 127–136 (2005).
 45. Ludtmann, M. H. et al. Monomeric alpha-synuclein exerts a physiological role on brain ATP synthase. *J. Neurosci.* **36**, 10510–10521 (2016).
 46. Ludtmann, M. H. R. et al. Alpha-synuclein oligomers interact with ATP synthase and open the permeability transition pore in Parkinson's disease. *Nat. Commun.* **9**, 2293 (2018).
 47. Liu, Z., Tang, C., Teng, X., Mohamed, Z. A. & Fan, J. Adenylate kinase 2 is a biomarker related to the prognosis of glioma and the immune microenvironment. *J. Clin. Lab Anal.* **37**, e24892 (2023).
 48. Garcia-Esparcia, P., Hernandez-Ortega, K., Ansoleaga, B., Carmona, M. & Ferrer, I. Purine metabolism gene deregulation in Parkinson's disease. *Neuropathol. Appl Neurobiol.* **41**, 926–940 (2015).
 49. Schiffrin, B. et al. Skp is a multivalent chaperone of outer-membrane proteins. *Nat. Struct. Mol. Biol.* **23**, 786–793 (2016).
 50. Li, D., Liu, M. S. & Ji, B. Mapping the dynamics landscape of conformational transitions in enzyme: the adenylate kinase case. *Biophys. J.* **109**, 647–660 (2015).
 51. Zhu, Y. et al. alpha-Synuclein overexpression impairs mitochondrial function by associating with adenylate translocator. *Int. J. Biochem Cell Biol.* **43**, 732–741 (2011).
 52. Song, K. et al. A convenient, rapid, sensitive, and reliable spectrophotometric assay for adenylate kinase activity. *Molecules.* <https://doi.org/10.3390/molecules24040663> (2019).
 53. Huang, C., Ren, G., Zhou, H. & Wang, C. C. A new method for purification of recombinant human alpha-synuclein in *Escherichia coli*. *Protein Expr. Purif.* **42**, 173–177 (2005).
 54. Schweighauser, M. et al. Structures of alpha-synuclein filaments from multiple system atrophy. *Nature* **585**, 464–469 (2020).
 55. Medeiros, J. et al. Partial magic angle spinning NMR (1)H, (13)C, (15)N resonance assignments of the flexible regions of a monomeric alpha-synuclein: conformation of C-terminus in the lipid-bound and amyloid fibril states. *Biomol. NMR Assign.* **15**, 297–303 (2021).
 56. Paslawski, W., Mysling, S., Thomsen, K., Jorgensen, T. J. & Otzen, D. E. Co-existence of two different alpha-synuclein oligomers with different core structures determined by hydrogen/deuterium

- exchange mass spectrometry. *Angew. Chem. Int. Ed. Engl.* **53**, 7560–7563 (2014).
57. Sidhu, A., Segers-Nolten, I., Raussens, V., Claessens, M. M. & Subramaniam, V. Distinct mechanisms determine alpha-synuclein fibril morphology during growth and maturation. *ACS Chem. Neurosci.* **8**, 538–547 (2017).
 58. Bonifati, V. et al. Mutations in the DJ-1 gene associated with autosomal recessive early-onset Parkinsonism. *Science* **299**, 256–259 (2003).
 59. Blackinton, J. et al. Formation of a stabilized cysteine sulfinic acid is critical for the mitochondrial function of the Parkinsonism protein DJ-1. *J. Biol. Chem.* **284**, 6476–6485 (2009).
 60. Pantcheva, P. et al. The role of DJ-1 in the oxidative stress cell death cascade after stroke. *Neural Regen. Res.* **9**, 1430–1433 (2014).
 61. Kriebel, G. et al. Reduced basal autophagy and impaired mitochondrial dynamics due to loss of Parkinson's disease-associated protein DJ-1. *PLoS One* **5**, e9367 (2010).
 62. Gao, H. et al. DJ-1 protects dopaminergic neurons against rotenone-induced apoptosis by enhancing ERK-dependent mitophagy. *J. Mol. Biol.* **423**, 232–248 (2012).
 63. Honbou, K. et al. The crystal structure of DJ-1, a protein related to male fertility and Parkinson's disease. *J. Biol. Chem.* **278**, 31380–31384 (2003).
 64. Reyes, J. F. et al. Accumulation of alpha-synuclein within the liver, potential role in the clearance of brain pathology associated with Parkinson's disease. *Acta Neuropathol. Commun.* **9**, 46 (2021).
 65. Kakimoto, T. et al. Accumulation of alpha-synuclein in hepatocytes in nonalcoholic steatohepatitis and its usefulness in pathological diagnosis. *Pathol. Res. Pr.* **247**, 154525 (2023).
 66. Moors, T. E. et al. Multi-platform quantitation of alpha-synuclein human brain proteoforms suggests disease-specific biochemical profiles of synucleinopathies. *Acta Neuropathol. Commun.* **10**, 82 (2022).
 67. Moors, T. E. et al. The subcellular arrangement of alpha-synuclein proteoforms in the Parkinson's disease brain as revealed by multi-color STED microscopy. *Acta Neuropathol.* **142**, 423–448 (2021).
 68. Ma, L. et al. C-terminal truncation exacerbates the aggregation and cytotoxicity of alpha-synuclein: a vicious cycle in Parkinson's disease. *Biochim. Biophys. Acta Mol. Basis Dis.* **1864**, 3714–3725 (2018).
 69. Zhang, C. et al. C-terminal truncation modulates alpha-synuclein's cytotoxicity and aggregation by promoting the interactions with membrane and chaperone. *Commun. Biol.* **5**, 798 (2022).
 70. Sorrentino, Z. A. & Giasson, B. I. The emerging role of alpha-synuclein truncation in aggregation and disease. *J. Biol. Chem.* **295**, 10224–10244 (2020).
 71. Anderson, J. P. et al. Phosphorylation of Ser-129 is the dominant pathological modification of alpha-synuclein in familial and sporadic Lewy body disease. *J. Biol. Chem.* **281**, 29739–29752 (2006).
 72. Tripathi, T. & Chattopadhyay, K. Interaction of alpha-synuclein with ATP synthase: switching role from physiological to pathological. *ACS Chem. Neurosci.* **10**, 16–17 (2019).
 73. Chung, C. Y. et al. In situ peroxidase labeling and mass-spectrometry connects alpha-synuclein directly to endocytic trafficking and mRNA metabolism in neurons. *Cell Syst.* **4**, 242–250 e244 (2017).
 74. Killinger, B. A. et al. In situ proximity labeling identifies Lewy pathology molecular interactions in the human brain. *Proc. Natl. Acad. Sci. USA.* **119**, e2114405119 (2022).
 75. Mas, G. et al. Regulation of chaperone function by coupled folding and oligomerization. *Sci. Adv.* **6**, eabc5822 (2020).
 76. Davis, J. B. & Maher, P. Protein kinase C activation inhibits glutamate-induced cytotoxicity in a neuronal cell line. *Brain Res.* **652**, 169–173 (1994).
 77. Beuster, G. et al. Inhibition of alanine aminotransferase in silico and in vivo promotes mitochondrial metabolism to impair malignant growth. *J. Biol. Chem.* **286**, 22323–22330 (2011).
 78. Frezza, C., Cipolat, S. & Scorrano, L. Organelle isolation: functional mitochondria from mouse liver, muscle and cultured fibroblasts. *Nat. Protoc.* **2**, 287–295 (2007).
 79. Barrientos, A. In vivo and in organello assessment of OXPHOS activities. *Methods* **26**, 307–316 (2002).
 80. Haraux, F. & Lombes, A. Kinetic analysis of ATP hydrolysis by complex V in four murine tissues: Towards an assay suitable for clinical diagnosis. *PLoS One* **14**, e0221886 (2019).
 81. Fernandez-Del-Rio, L. et al. A novel approach to measure complex V ATP hydrolysis in frozen cell lysates and tissue homogenates. *Life Sci. Alliance.* <https://doi.org/10.26508/lsa.202201628> (2023).
 82. Perez-Riverol, Y. et al. The PRIDE database at 20 years: 2025 update. *Nucleic Acids Res.* **53**, D543–D553 (2025).

Acknowledgements

We thank Dr. Ludovic Gillet (ETH Zurich) for fruitful discussions. We thank Dr. Lukas Frey (ETH Zurich) for the assistance with the design of the graphical illustrations. This study was supported by a Sinergia grant from the Swiss National Science Foundation (CRSII5_177195 to P.P. and R.R.); by grants from Parkinson Schweiz (to P.P.); by the Synapsis Foundation—Alzheimer Research Switzerland (to P.P. and 2023-CDA02 to T.S.); by the Gelu Foundation (to T.S.); and by the Swiss National Science Foundation (205321_192409/1, to L.M.).

Author contributions

Conceptualization: T.S., Y.F., P.P. and R.R. Methodology: T.S., V.R. and P.P. (structural proteomics), Y.F., L.F., and R.R. (NMR), D.G., Y.F., G.M., S.H., L.K., and R.R. (protein purification), Y.F., A.D., L.M., R.S., and R.R. (mitochondria isolation), Y.F., A.D., D.G., J.G., L.M., R.S. and R.R. (functional and aggregation assays), D.R. (transmission electron microscopy), V.R., T.S. and P.P. computational predictions. Data analysis: T.S., Y.F., R.R., and P.P. (overall experiments), A.D., L.M. and R.S. (ATP production). N.V. and C.D. contributed to the experimental setup. Supervision: R.R. and P.P. Writing: Y.F., T.S., P.P. and R.R. All authors reviewed, edited, and approved.

Competing interests

Paola Picotti is a scientific advisor for the company Biognosys AG (Zurich, Switzerland) and an inventor of a patent licensed by Biognosys AG that covers the LiP-MS method used in this manuscript. All other authors declare no competing interests.

Additional information

Supplementary information The online version contains supplementary material available at <https://doi.org/10.1038/s41467-025-62895-4>.

Correspondence and requests for materials should be addressed to Paola Picotti or Roland Riek.

Peer review information *Nature Communications* thanks Tara Pukala and the other anonymous reviewer(s) for their contribution to the peer review of this work. A peer review file is available.

Reprints and permissions information is available at <http://www.nature.com/reprints>

Publisher's note Springer Nature remains neutral with regard to jurisdictional claims in published maps and institutional affiliations.

Open Access This article is licensed under a Creative Commons Attribution-NonCommercial-NoDerivatives 4.0 International License, which permits any non-commercial use, sharing, distribution and reproduction in any medium or format, as long as you give appropriate credit to the original author(s) and the source, provide a link to the Creative Commons licence, and indicate if you modified the licensed material. You do not have permission under this licence to share adapted material derived from this article or parts of it. The images or other third party material in this article are included in the article's Creative Commons licence, unless indicated otherwise in a credit line to the material. If material is not included in the article's Creative Commons licence and your intended use is not permitted by statutory regulation or exceeds the permitted use, you will need to obtain permission directly from the copyright holder. To view a copy of this licence, visit <http://creativecommons.org/licenses/by-nc-nd/4.0/>.

© The Author(s) 2025